NASA Contractor Report 3074

Development of a Digital Guidance and Control Law for Steep Approach Automatic Landings Using Modern Control Techniques

Nesim Halyo

CONTRACT NAS1-14088
FEBRUARY 1979

NASA

NASA Contractor Report 3074

Development of a Digital Guidance and Control Law for Steep Approach Automatic Landings Using Modern Control Techniques

Nesim Halyo
Analytical Mechanics Associates, Inc.
Hampton, Virginia

Prepared for
Langley Research Center
under Contract NAS1-14088

National Aeronautics
and Space Administration

Scientific and Technical
Information Office

1979

TABLE OF CONTENTS

LIST OF FIGURES

LIST OF TABLES

I. INTRODUCTION

With the high accuracy of guidance information provided by the Microwave Landing System (MLS), the use of curved flight paths and steep glideslopes in the final approach in terminal areas has become possible. As the Microwave Landing System is less sensitive to weather conditions than conventional systems, automatic landing systems using the MLS can be used to reduce the congestion in terminal areas due to adverse weather conditions. To meet projected aviation requirements through optimum utilization of the MLS and "state of the art" guidance and control technology, NASA has introduced the Terminal Configured Vehicle (TCV) Program at the Langley Research Center, [1]. The goals of the TCV Program include the reduction of aircraft noise in airport communities, all-weather operation in the terminal area, and the efficient utilization of airspace in congested terminal areas.

The Microwave Landing System is a ground-based guidance system under development by the FAA, which provides position information to aircraft within its volumetric coverage [2]. It consists of a DME providing range information, an azimuth antenna generally collocated with the DME antenna providing the aircraft's azimuth angle relative to the runway centerline up to $\pm 60^{\circ}$, and an elevation antenna located at the glidepath intercept point but offset to the side of the runway providing the aircraft's elevation angle up to 20°. The MLS thus has a volumetric coverage, and provides guidance information that can be used for steep approaches and curved flight paths in the terminal area.

This work considers the development of a digital automatic control law for the TCV research aircraft (B-737) to perform a steep final approach in automatic landings. The use of a steep glideslope in the final approach reduces the intensity of the noise perceived on the ground, provides a method to avoid the vortex generated by a large aircraft flying a shallower glideslope, and provides more flexibility in sequencing and spacing of aircraft at different altitudes, thus allowing more efficient use of airspace. A 3D, constant airspeed control law which engages at localizer capture and brings the aircraft to touchdown was developed for the lateral and longitudinal dynamics. Localizer and glideslope capture can be engaged simultaneously, resulting in a curved capture path horizontally as well as vertically.

A decrab law with a maximum roll of 5° is used to control the effects of crosswinds in landings. The flare law was developed to follow a fixed flare path in order to reduce touchdown dispersion under varying wind conditions in steep approaches. The control system uses MLS position data and body-mounted accelerometer data in place of inertial platform accelerations, which are filtered along with attitude and body rate information. The filter provides less noisy estimates of the data obtained by the instruments as well as estimates of non-measured parameters such as the sideslip angle and wind velocities. These filtered outputs are then used to control the aircraft during the final approach. The control law considers the localizer capture, glideslope capture, steep glideslope tracking, and flare to touchdown phases of flight and includes a decrab law for automatic landings where a crosswind is present. The control law was developed using modern digital optimal control techniques which are well-suited to the discrete character of the Microwave Landing System.

In Section II, the aircraft's equations of motion and the wind model are described. A perturbation model of the aircraft's lateral dynamics for a steep glideslope of 6° is obtained and is expressed in state variable form. Using the Dryden spectrum, a dynamical model for the simulation of wind gusts affecting the aircraft's lateral dynamics is developed. Then steady winds and shear are included into the wind model.

In Section III, a mathematical model for the noises in the various on-board sensors and a model for the noisy MLS data are developed for simulation purposes. The development of the filter equations is then described.

In Section IV, the development of a digital automatic control law for the lateral dynamics of the aircraft and a constant airspeed, 3D control law for the longitudinal dynamics is described. The control uses the filtered estimates of measured variables as well as wind velocity estimates to control the aircraft's deviations from runway centerline and the glideslope during the final approach.

In Section V, the results obtained from a digital simulation of the aircraft dynamics, wind conditions, sensor noises using the control law and filter developed are described.

II. MODEL OF THE AIRCRAFT DYNAMICS AND WIND CONDITIONS

In this section, mathematical models for the lateral and longitudinal (including vertical) dynamics of the aircraft and the wind components which have an effect on the aircraft's dynamics will be developed. The models developed will be used in the digital simulation of the motion of the aircraft under different wind conditions and in the development of the filtering algorithm and the automatic control law. The equations thus obtained will then be expressed in state variable form which is more suitable for the application of modern optimal control techniques. The control law developed will then be evaluated using a non-linear model of the aircraft dynamics.

A. MODEL OF THE LATERAL DYNAMICS

To simulate the motion of the aircraft on a digital computer, a mathematical model is necessary. The general equations of motion for aircraft are non-linear differential equations where the longitudinal and lateral motion variables are coupled [3], [4], [5]. However, under a steady flight condition assumption, these equations can be simplified significantly with little change in their validity [3, pp. 154-165], [4, p. 2.30]. In the development presented here, the phases of the final approach considered are the localizer capture, glideslope capture, glideslope tracking and flare. With the exception of localizer capture, in the phases of flight considered the roll, yaw and pitch angles have quite small values, where the yaw angle is measured relative to runway centerline; thus, with a constant airspeed, a steady flight condition would be present. During localizer capture, the yaw angle may have large values. Similarly, the roll angle may also have large values during capture; however, as the time period over which large values in the roll angle would be sustained is relatively short, this would not invalidate the simplified equations of motion. On the other hand, the yaw angle does not affect the values of the stability derivatives in any given flight condition. This is due to the fact that roughly the yaw angle describes the angular deviation of the body x-axis from the runway centerline, whereas the stability derivatives

depend on the values of aerodynamic variables such as the sideslip angle, angle of attack, etc., which describe the motion of the aircraft relative to the atmosphere surrounding it. The yaw angle is used, however, in the computations of the aircraft's position and velocity relative to an earth-fixed coordinate frame; i.e., in transforming body-axis variables into inertial variables. Thus, for large values of yaw, the small angle approximation in the transformation from say stability axes to earth-fixed axes does not hold and these transformations have to be dealt with separately.

When the steady-state body attitude rates, the steady-state velocity component along the body y-axis and the steady-state bank angle have a value of zero, the general equations of motion can be linearized to obtain the perturbation equations, where the longitudinal and lateral variables are no longer coupled (e.g., see [2], p. 2.33).

$$m(\dot{v} + U_o r - W_o p) = mg \cos\gamma_o \varphi + f_{Ay} + f_{Ty} \quad , \tag{1}$$

$$I_{xx}\dot{p} - I_{xz}\dot{r} = \ell_A + \ell_T \quad , \tag{2}$$

$$I_{zz}\dot{r} - I_{xz}\dot{p} = n_A + n_T \quad . \tag{3}$$

Equations (1) - (3) are the perturbation equations which describe the lateral dynamics of the aircraft, where

U_o - steady-state inertial speed along the stability x-axis, i.e. along x_s ,

W_o - steady-state inertial speed along the stability z-axis, i.e. along z_s ,

v - perturbation in the inertial speed along the stability y-axis, i.e. along y_s ,

p - perturbation in the roll rate about x_s ,

r - perturbation in the yaw rate about z_s ,

γ_o - steady-state flight path angle,

φ - perturbation in the roll angle,

f_{Ay} - perturbation in the net aerodynamic force along y_s ,

f_{Ty} - perturbation in the thrust force along y_s ,

ℓ_A - perturbation in the rolling moment due to aerodynamic forces,

n_A - perturbation in the yawing moment due to aerodynamic forces,

ℓ_T - perturbation in the rolling moment due to thrust,

n_T - perturbation in the yawing moment due to thrust,

and I_{xx}, I_{zz} and I_{xz} are the moments of inertia of the aircraft in the stability axes.

Now, the terms f_{Ay}, f_{Ty}, ℓ_A, ℓ_T, n_A and n_T can be expressed in terms of the stability derivatives of the aircraft evaluated at the steady state values of the aerodynamic variables and the control surface settings, in linear form [3], [4], [5]. Substituting these expressions into equations (1) - (3) and rearranging terms we obtain linear differential equations in the sideslip angle, the roll rate and yaw rate. Writing the derivatives of the roll and yaw angles in terms of roll and yaw rates, we obtain the following set of differential equations.

$$\dot{\varphi} = \sec\theta_o (\cos\gamma_o\, p + \cos\gamma_o\, r) \tag{4}$$

$$\dot{\psi} = \sec\theta_o (\sin\alpha_o\, p + \cos\alpha_o\, r) \tag{5}$$

$$\begin{aligned}\dot{\beta} = {} & a_{31}\, \varphi + a_{33}\, \beta + a_{34}\, p + a_{35}\, r + b_{31}\, \delta A + b_{32}\, \delta R \\ & + b_{33}\, \delta sp + h_{31}\, \beta_W + h_{32}\, p_W + h_{33}\, r_W\end{aligned} \tag{6}$$

$$\begin{aligned}\dot{p} = {} & a_{43}\, \beta + a_{44}\, p + a_{45}\, r + b_{41}\, \delta A + b_{42}\, \delta R + b_{43}\, \delta sp \\ & + h_{41}\, \beta_W + h_{42}\, p_W + h_{43}\, r_W\end{aligned} \tag{7}$$

$$\begin{aligned}\dot{r} = {} & a_{53}\, \beta + a_{54}\, p + a_{55}\, r + b_{51}\, \delta A + b_{52}\, \delta R + b_{53}\, \delta sp \\ & + h_{51}\, \beta_W + h_{52}\, p_W + h_{53}\, r_W\end{aligned} \tag{8}$$

where β, p and r are the sideslip angle, roll rate and yaw rate relative to the inertial frame of reference, respectively, β_W, p_W and r_W are the sideslip angle, the roll rate and yaw rate due to wind velocities only, δA, δR and δsp are the perturbations of the ailerons, rudder and spoilers, respectively. The coefficients

a_{ij} in the above equations depend on the aircraft stability derivatives and are given in the Appendix. Thus, a set of linear differential equations describing the lateral velocities and attitude of the aircraft can be obtained.

The position of the aircraft relative to runway centerline is expressed by the perpendicular distance of the aircraft center of mass to the runway centerline. This distance normalized by the aircraft's steady state speed will be used as a state variable in addition to the equations already obtained. Thus, let L_{ES} be the matrix representing the transformation from the aircraft stability axes to the earth-fixed axes; so that L_{ES} (i, j) is the element in the ith row and j^{th} column of the matrix. Then, the lateral distance y (in feet) of the aircraft can be expressed by

$$\dot{y} = U_o\left[L_{ES}(2, 1)(1 + u') + L_{ES}(2, 2)\beta + L_{ES}(2, 3)\alpha \right], \qquad (9)$$

where u' is the normalized inertial perturbation in the speed along the x_s direction and α is the perturbation in the inertial angle of attack, and

$$L_{ES}(2, 1) = \cos\alpha_o \cos\theta \sin\psi + \cos\varphi \sin\alpha_o \sin\theta \sin\psi - \sin\alpha_o \sin\varphi \cos\psi \qquad (10)$$

$$L_{ES}(2, 2) = \sin\varphi \sin\theta \sin\psi + \cos\varphi \cos\psi \qquad (11)$$

$$L_{ES}(2, 3) = -\sin\alpha_o \cos\theta \sin\psi + \cos\alpha_o \cos\varphi \sin\theta \sin\psi - \cos\alpha_o \sin\varphi \cos\psi \,. \qquad (12)$$

Rearranging the terms in equation (9)

$$\dot{y}' = \beta + \cos(\alpha_o - \theta_o)\,\psi - \sin\alpha_o\,\varphi + \eta_y \,, \qquad (13)$$

where η_y and y' are given by

$$\eta_y = (L_{ES}(2, 2) - 1)\beta + L_{ES}(2, 1)(1 + u') - \cos(\alpha_o - \theta_o)\,\psi + L_{ES}(2, 3)\alpha + \sin\alpha_o\,\varphi \,, \qquad (14)$$

$$y' = y/U_o \,. \qquad (15)$$

Note that equation (13) contains no approximation when α is interpreted as the normalized inertial velocity component in the z_s direction, but is simply a rearranged form of (9) with the non-linear terms grouped into a single term.

The controls which affect the lateral motion of the aircraft are the aileron, rudder and spoiler surface settings as can be seen from equations (4) - (8), where the spoiler action is used only to aid the effect of the ailerons during turns. Thus, the spoiler setting is programmed according to the aileron setting and is modelled here as

$$\delta s_p = C_{spa} \; \delta A \quad , \qquad C_{spa} = 1.73 \; . \tag{16}$$

To further account for the relatively slow motion of the rudder, a rate command is preferred to a position command; hence, the rudder position is considered a state variable which is obtained by integrating the rudder rate command.

$$\dot{\delta R} = u_3 \; , \tag{17}$$

where u_3 is considered to be the rudder rate control.

If the relation between the spoiler and aileron given in (16) is substituted into (6), (7) and (8), then the spoiler terms are eliminated from the equations. Now, forming a state vector x such that

$$x^T = (\varphi \quad \psi \quad \beta \quad p \quad r \quad y' \quad \delta R) \tag{18}$$

and a control vector u such that

$$u^T = (\delta A \quad \dot{\delta R}) \; , \tag{19}$$

equations (4) - (8), (13), (16) and (17) can be combined into a state variable model of the lateral motion of the aircraft of the form,

$$\dot{x} = Ax + Bu + Dw + \bar{\eta} , \tag{20}$$

where $w^T = (\beta_w \quad p_w \quad r_w)$ and $\bar{\eta}^T = (0 \quad 0 \quad 0 \quad 0 \quad 0 \quad \eta_y \quad 0)$.

Thus, equation (20) describes the lateral motion of the aircraft when the aircraft is controlled by the surface settings of the ailerons and rudder in the state variable format. The effect of winds on the motion is also included through the term w.

B. MODEL OF LONGITUDINAL DYNAMICS

The longitudinal equations, which describe the motion of the aircraft in the forward and vertical directions, can be obtained using a similar treatment as the lateral equations of motion. As noted in the last section, for the phases of flight considered in this work, the equations of motion can be described as perturbations about a steady flight condition where the longitudinal and lateral variables are uncoupled. Further, the pitch angle and the angle of attack are usually small enough to allow the use of small angle approximations. Thus, the longitudinal equations of motion can be described by linear differential equations in the perturbations from the steady flight condition as shown below [3].

$$m\dot{u} = mg\cos\gamma_o\,\theta_p + \bar{q}_o S\Big[(-C_{Du'} + 2C_{D_o} + C_{Tx_{u'}} + 2C_{Tx_o})\,\underline{u'} + (C_{Lo} - C_{D\alpha})\,\underline{\alpha} - C_{D\delta e}\,\delta e - C_{D\delta s}\,\delta s + C_{Tx\delta T}\,\delta T\Big] \tag{21}$$

$$m(\dot{w} - U_o q) = -mg\sin\gamma_o\,\theta_p + \bar{q}_o S\Big[-(C_{Lu'} + 2C_{Lo})\,\underline{u'} - (C_{L\alpha} + C_{Do})\,\underline{\alpha} - C_{L\dot{\alpha}}\,\dot{\underline{\alpha}} - C_{Lq}\,\underline{q}\Big] \tag{22}$$

$$I_{yy}\,\dot{q} = \bar{q}_o S\Big[(C_{Mu'} + 2C_{Mo})\,\underline{u'} + (C_{M\alpha} + C_{MT\alpha})\,\underline{\alpha} + C_{M\dot{\alpha}}\,\dot{\underline{\alpha}} + C_{Mq}\,\underline{q} + C_{M\delta e}\,\delta e + C_{M\delta s}\,\delta s + C_{M\delta T}\,\delta T\Big], \tag{23}$$

where,

$$\underline{u'} = u' + u'_w,\quad u' = \frac{u}{U_o},\quad u'_w = \frac{u_w}{U_o}, \tag{24}$$

$$\underline{\alpha} = \alpha + \alpha_w,\quad \alpha = \frac{w}{U_o}, \tag{25}$$

$$\underline{q} = q + q_w, \tag{26}$$

$$\theta_p = \theta - \theta_o, \tag{27}$$

u and α are the perturbations in the inertial speed along the x stability axis and the inertial angle of attack, respectively, q is the pitch rate, u_w , α_w and q_w are the components due to winds, $\bar{q}o$ is the steady state value of the dynamic pressure, S is the effective wing area, δe, δs and δT are the perturbations in the elevator, stabilizer and thrust from their steady values, respectively. A more detailed derivation of the longitudinal equations of motion used here is given in [10], [11].

The position of the aircraft relative to the earth-fixed coordinate frame can be obtained by integrating the inertial velocity components along each coordinate; thus,

$$\dot{x}' = \frac{\dot{x}}{U_o} = L_{ES}(1, 1)(1 + u') + L_{ES}(1, 2)\beta + L_{ES}(1, 3)\alpha , \qquad (28)$$

$$\dot{z}' = \frac{\dot{z}}{U_o} = L_{ES}(3, 1)(1 + u') + L_{ES}(3, 2)\beta + L_{ES}(3, 3)\alpha . \qquad (29)$$

Note that α and β are inertial quantities and correspond to normalized velocity components in the stability axes; under no wind conditions these would be the same as the aerodynamic angle of attack and sideslip. We can rewrite the position equations in the following form.

$$\dot{x}' = -\sin\gamma_o\,\theta_p + \cos\gamma_o\,u' + \sin\gamma_o\,\alpha + \eta_x , \qquad (30)$$

$$\dot{z}' = -\cos\gamma_o\,\theta_p - \sin\gamma_o\,u' + \cos\gamma_o\,\alpha + \eta_z , \qquad (31)$$

where

$$\eta_x = L_{ES}(1, 1)(1 + u') - \cos\gamma_o\,u' + \sin\gamma_o\,\theta_p + L_{ES}(1, 2)\beta + (L_{ES}(1, 3) - \sin\gamma_o)\alpha , \qquad (32)$$

$$\eta_z = L_{ES}(3, 1)(1 + u') + \sin\gamma_o\,u' + \cos\gamma_o\,\theta_p + L_{ES}(3, 2)\beta + (L_{ES}(3, 3) - \cos\gamma_o)\alpha . \qquad (33)$$

In this form, the differential equations are linear with a forcing function that contains the non-linear part which are second order terms with respect to the steady flight condition considered. With this approach we can use linear

theory in the development of the filter and control law without neglecting the non-linear terms completely.

To account for the effects of the servo responses for the stabilizer and engine dynamics, simple linear models were used.

$$\delta \dot{T} = -.5\,\delta T + .298\,\delta th \quad , \tag{34}$$

$$\delta \dot{th} = u_3 \quad , \tag{35}$$

$$\delta \dot{s} = u_2 \quad , \tag{36}$$

where δT is the thrust perturbation in units of one thousand pounds per unit of δT, δth is the throttle perturbation in degrees and δs is the stabilizer perturbation in radians. As the lags in the elevator action are small, the elevator time constant was neglected. The aircraft's longitudinal equations of motion, the position equations and the actuator equations can be combined and after some manipulation can be expressed in state variable form.

$$x_\ell^T = (\theta_p \quad u' \quad \alpha \quad q \quad x' \quad z' \quad \delta T \quad \delta th \quad \delta s) \quad ,$$

$$u_\ell^T = (\delta e \quad \delta \dot{s} \quad \delta \dot{th}) \quad ,$$

$$w_\ell^T = (u'_w \quad \alpha_w \quad q_w) \quad ,$$

$$\eta_\ell^T = (0 \quad 0 \quad 0 \quad 0 \quad \eta_x \quad \eta_z \quad 0 \quad 0 \quad 0) \quad ,$$

$$x_\ell = A_\ell x_\ell + B_\ell u_\ell + D_\ell w_\ell + \eta_\ell \quad , \tag{37}$$

where A_ℓ, B_ℓ, and D_ℓ are matrices of appropriate size corresponding to the coefficients in the original equations. Expressions for the elements of these matrices can be obtained in terms of the stability derivatives of the aircraft.

C. MODEL OF THE WIND CONDITIONS

The lateral motion of the aircraft is described by the state variable model given in equation (20); this model describes the response of the aircraft when a control is applied or when the wind velocities such as gusts or steady winds are non-zero. The effects of the wind velocities are introduced through the vector w. The components of this vector are β_W or the wind velocitiy along the y_S direction normalized by the airspeed of the aircraft, p_W or the rotation of the air around the aircraft about the x_S axis, and r_W or the rotation of the air around the aircraft about the z_S axis, respectively. The roll rate p_W and yaw rate r_W components of the wind vector w consist only of the effects of wind gusts, thus having an average value of zero; i. e., these components do not have a steady state effect but introduce turbulence effects into the equations. On the other hand, the β_W or the normalized lateral wind velocity contains terms for both wind gusts and steady winds; thus,

$$\beta_W = \beta_g + \beta_S \quad , \tag{38}$$

where β_g is the gust or turbulence term, and β_S is the steady wind term. The gust terms are of a random nature and can be modelled using the well-known Dryden spectrum [3] , [4]. This method consists of using spectral factorization methods to obtain a dynamical system which generates a random process having the specified power spectral density when driven by a white noise process [6], [7], [8].

The Dryden spectra describe the statistical behaviour of wind gust velocities along the aircraft body coordinates by specifying their power spectral densities in terms of the spatial frequency Ω [9]. The spectra for the gust components of interest are given below.

$$\varphi_\beta(\Omega) = \sigma_v^2 \frac{Lv}{\pi V^2} \frac{1 + 3\,(L_v\,\Omega)^2}{[\,1 + (L_v\,\Omega)^2\,]^2} \quad , \tag{39}$$

$$\varphi_p(\Omega) = \frac{\sigma_w^2}{L_w} \frac{.8\left(\frac{\pi L_w}{4b}\right)^{\frac{1}{3}}}{1 + \left(\frac{4b\,\Omega}{\pi}\right)^2} \tag{40}$$

$$\varphi_r(\Omega) = \frac{\Omega^2 V^2}{1 + \left(\frac{3b\,\Omega}{\pi}\right)^2} \varphi_\beta(\Omega) \quad , \tag{41}$$

where b is the wing span, L_v and L_w are the scales of turbulence, V is the airspeed, σ_v^2 is the variance of the lateral gust and σ_w^2 is the variance of the vertical gust. The change from the spatial frequency Ω to the temporal frequency ω can be made by

$$\Omega = \frac{\omega}{V} \quad . \tag{42}$$

Substituting equation (42) into the expressions for the power spectral densities of the wind gusts we obtain the spectra in terms of the temporal frequency; then using spectral factorization techniques the following transfer functions can be obtained

$$H_\beta(s) = -\sigma_v \left[\frac{L_v}{\pi V^3}\right]^{\frac{1}{2}} \frac{1 + \frac{3 L_v s}{V}}{\left(1 + \frac{L_v s}{V}\right)^2} \quad , \tag{43}$$

$$H_p(s) = \sigma_w \left[\frac{1}{L_w V}\right]^{\frac{1}{2}} \frac{\left[.8\left(\frac{\pi L_w}{4b}\right)^{\frac{1}{3}}\right]^{\frac{1}{2}}}{1 + \frac{4b\,s}{\pi V}} \quad , \tag{44}$$

$$H_r(s) = \frac{-s}{1 + \frac{3b\,s}{\pi V}} H_\beta(s) \quad . \tag{45}$$

It should be noted that even though p_w is independent of β_w and r_w , the latter two are not independent of each other Thus, if a white noise process is input to the transfer function $H_r(s)$, the output would have the desired power spectral density, but may not have the desired cross-correlation with

β_g. Hence, equation (45) must be interpreted as β_g being the input to the first term in the above equation in order that the proper cross-correlation be obtained.

The wind gust terms can thus be simulated by passing white noise through the systems with the transfer functions given in equations (43), (44), and (45). The lateral wind, however, has a steady or average value which is not necessarily negligible. Thus, consider that a steady wind is present; in the earth-fixed coordinate system, the wind velocity has a component in the direction of runway centerline W_X, and a component perpendicular to the runway centerline say W_5; it is assumed that there is no steady wind in the vertical direction although gusts may be present. Hence, if L_{SE} is the transformation matrix from earth-fixed to stability coordinates, then the steady component, β_s, of the normalized lateral wind velocity is given by

$$\beta_s = L_{SE}(2, 2)\ W_5 + L_{SE}(2, 1)\ W_X \quad , \tag{46}$$

$$L_{SE}(2, 1) = \sin\theta \sin\varphi \cos\psi - \cos\varphi \sin\psi \quad , \tag{47}$$

$$L_{SE}(2, 2) = \sin\theta \sin\varphi \sin\psi + \cos\varphi \cos\psi \quad . \tag{48}$$

To include wind shear into the model, the steady lateral wind velocity can be described as

$$\dot{W}_5 = W_6 + \omega_3 \quad , \tag{49}$$

$$\dot{W}_6 = \omega_4 \quad , \tag{50}$$

where ω_3 and ω_4 are gaussian white noise processes independent of each other and of β_g, p_W and r_W. Now, the transfer functions for the gusts described in (43), (44), and (45) can be combined into a state variable model of fourth order. Adding (49) and (50) to this model we obtain a sixth order model of the form

$$\dot{W} = A_W\ W + B_W\ \omega \quad , \tag{51}$$

where W_1 is β_g , W_3 is r_W , W_4 is p_W , ω is a 4-vector of independent gaussian white noise processes, and A_W , B_W are given in the Appendix. Thus, the wind vector W can be generated using equation (51). To complete the development of wind conditions the vector w is needed for substitution into (20); this vector can be obtained from W as follows. First note that the elements of w are in the stability axes; hence, W_3 and W_4 must be transformed from body to stability axes; then the steady winds must also be expressed in this coordinate system. Thus, we obtain

$$\beta_W = W_1 + W_5 + \xi_1 \quad , \tag{52}$$

$$p_W = \sin \alpha_0 \; W_3 + \cos \alpha_0 \, W_4 \quad , \tag{53}$$

$$r_W = \cos \alpha_0 \; W_3 - \sin \alpha_0 \, W_4 \quad , \tag{54}$$

where $\xi_1 = (L_{SE} (2, 2) - 1) \; W_5 + L_{SE} (2, 1) \; W_X$.

These equations can be expressed in matrix notation as

$$w = C_W \; W + \xi \quad , \tag{55}$$

where ξ is a vector with its first element ξ_1 as given above and its other two elements zero. Thus W can be generated using (51), and w given in (55) can be substituted into (20) to simulate the effects of a given wind condition on the motion of the aircraft; hence,

$$\dot{x} = Ax + Bu + DC_W \; W + \eta \; , \quad \eta = D\xi + \bar{\eta} \quad , \tag{56}$$

$$\dot{W} = A_W \; W + B_W \, \omega \quad . \tag{57}$$

The longitudinal wind model contains the components of steady wind velocities, turbulence and shear winds in the longitudinal axis. The turbulence model uses the Dryden spectra [4] for the various components varying with altitude. The turbulence model has three components: u'_g in the x_b direction, α_g in the z_b

direction, and q_g which models the effect of turbulence on the pitch rate of the aircraft. These components are modelled using the following spectra.

$$S_u(\Omega) = \frac{2\sigma_u^2 L_u}{1 + (L_u \Omega)^2} , \tag{58}$$

$$S_\alpha(\Omega) = \frac{\sigma_w^2 L_w}{Va^2} \frac{1 + 3(L_w\Omega)^2}{[1 + (L_w\Omega)^2]^2} , \tag{59}$$

$$S_q(\Omega) = \frac{\Omega^2 Va^2}{1 + (\frac{4b}{\pi}\Omega)^2} S_\alpha(\Omega) , \tag{60}$$

where b is the wing span, L_u and L_w are the scales of turbulence, Va is the airspeed, and Ω is the spatial frequency related to the temporal frequency ω by

$$\Omega = \omega / Va . \tag{61}$$

The u'_g component is independent of α_g and q_g, however, α_g and q_g are correlated with their cross spectral density being

$$S_{q\alpha}(\omega) = \frac{j\omega}{1 + j\frac{4b}{\pi Va}\omega} S_\alpha(\omega) . \tag{62}$$

The above spectra can be factored using spectral factorization methods to obtain a linear system driven by white noise which generates an output having the above spectral characteristics [6], [7], [8]. Thus, the following transfer functions are obtained to generate u'_g, α_g and q_g.

$$G_u(s) = \frac{1}{1 + \frac{L_u}{Va} s} , \tag{63}$$

$$G_\alpha(s) = \frac{1 + \sqrt{3}\frac{L_w}{Va} s}{1 + 2\frac{L_w}{Va} s + (\frac{L_w}{Va})^2 s^2} , \tag{64}$$

$$G_q(s) = \frac{s}{1 + \frac{4b}{\pi Va} s} , \tag{65}$$

where α_g is the input to the system G_q (s) to obtain q_g with the specified spectrum and cross-spectral density. Figures 1 and 2 show a block diagram of the system generating the turbulence components.

The steady and shear wind in the longitudinal direction was modelled by

$$\dot{u}'_s = u'_{sh} \quad , \qquad \dot{u}'_{sh} = \xi_{\ell 3} \quad , \tag{66}$$

$$\dot{\alpha}_s = \xi_{\ell 4} \quad . \tag{67}$$

Thus, to simulate a specified shear profile for $\dot{u}'_s$, with appropriate initial conditions, e.g., to obtain a linear profile u'_s changing at a rate of u'_{sho} , the initial condition for u'_{sh} is set to u'_{sho} and $\xi_{\ell 3}$ is set equal to zero; alternately, an impulse in $\xi_{\ell 3}$ will also achieve the same profile.

The transfer functions obtained for the wind model can equivalently be expressed as differential equations in state variable form as shown in (68) ; the matrices $A_{w\ell}$, $B_{w\ell}$ and $C_{w\ell}$ are given in the Appendix.

$$\dot{W}_\ell = A_{w\ell} \; W_\ell + B_{w\ell} \; \xi_\ell \, , \quad w_\ell = C_{w\ell} \; W_\ell \quad , \tag{68}$$

where w_ℓ is given by equation (37).

III. DEVELOPMENT OF FILTER EQUATIONS

This section describes the development of the filtering equations which are used with the longitudinal and lateral control laws during the final approach. The filters are used to reduce the noise in the various sensors and to obtain estimates of parameters which are not directly measured such as the wind velocities. As the Microwave Landing System (MLS) provides high accuracy position data to the aircraft at discrete points in time, a digital design was considered appropriate for the filtering function; this is also suitable for implementation on a digital computer such as the mini-computers on board the TCV aircraft. Furthermore, the performance of an analog (or continuous) filter implemented on a digital computer generally degrades as the sampling period or the integration step size increases, thus requiring a relatively high update rate, and computation time. The use of a digital design allows the choice of error feedback gains which take the sampling period into account as a constraint; thus reducing the degradation in performance. The form of filter used was a Kalman filter with constant gain; the steady state Kalman gains were used as a starting point to adjust the gains for good performance.

A. MLS AND SENSOR MODELS

The aircraft's position is obtained using the MLS guidance system, which provides volumetric coverage in the terminal area. The aircraft receives range, azimuth and elevation information at discrete intervals from which it can obtain its position with high accuracy even under adverse weather conditions. The ground azimuth antenna is located at the runway centerline past the end of the runway; thus it provides the aircraft with its azimuth angle relative to runway centerline up to $\pm 60^{\circ}$. The DME antenna which provides the range of the aircraft is generally co-located with the azimuth antenna. If the DME is located to the side of the runway, a simple transformation can still be used to obtain the aircraft's position. The elevation antenna is located at the glidepath intercept point (GPIP), but is offset to the side of the runway; it provides the aircraft's elevation angle up to 20°. Thus, the aircraft has accurate position information in the volume of space within the limits mentioned above.

Consider a right handed coordinate frame with its origin at the phase center of the azimuth antenna, the x-axis along runway centerline and positive towards the runway, and the z-axis positive vertically upwards. Then if the position of the aircraft in this coordinate system (the MLS coordinate frame) is (x_o, y_o, z_o), then the MLS signals would have the values given by the formulas below.

$$R = \sqrt{x_o^2 + y_o^2 + z_o^2} \quad , \tag{69}$$

$$Az = \sin^{-1} \frac{-y_o}{R} \quad , \tag{70}$$

$$El = \tan^{-1} \frac{z_o}{\sqrt{(x_o - x_e)^2 + (y_o - y_e)^2}} \quad , \tag{71}$$

where x_e and y_e are the x and y coordinates of the elevation antenna phase center in the MLS coordinate frame. The MLS signals received on the airplane are simulated with additive white noise, bias and jitter.

The onboard sensors used are three body-mounted accelerometers, attitude gyros for the pitch, roll and yaw angles, attitude rate gyros, barometric altitude and sink rate, airspeed and radar altitude. The accelerometers are mounted so as to measure the specific force along the aircraft's body axes. Let L_{BE} be the matrix which transforms a vector from earth-fixed coordinates to body-axis coordinates, and L_{AB} the matrix transformation from body-axis coordinates to the actual accelerometer axis; i.e., it is assumed that the accelerometers are misaligned and are not exactly parallel to the aircraft's body-axes. Then the accelerometer reading, F, is modelled as

$$F = L_{AB} f_B + b_a + n_a \quad , \tag{72}$$

$$f_B = a_B - L_{BE} g \quad , \tag{73}$$

where a_B is the acceleration vector in body axes, f_B the specific force vector in body axes, b_a the bias vector, n_a the noise vector and g is the gravity vector in the earth-fixed coordinate frame, given by

$$g^T = (0 \quad 0 \quad 32.2) \quad . \tag{74}$$

The earth-fixed coordinate frame is a right-handed coordinate frame with its origin at the GPIP on runway centerline, the x-axis positive toward the azimuth antenna, and the z-axis positive vertically downward.

The attitude gyros for the pitch, roll and yaw angles are modelled as having an additive bias and additive white noise. The attitude rate gyros do not have a bias error but are modelled as being corrupted by additive white noise. The barometric altitude and radar altitude measurement errors are modelled by additive bias and additive white noise. On the other hand, the barometric sink rate and airspeed measurement errors are modelled by multiplicative noise. Thus, if V_m is the measured airspeed, then

$$V_m = (1 + e)\ V \quad , \tag{75}$$

where V is the aircraft's airspeed and e is a zero mean white noise process.

At high altitudes, the radar altitude accuracy is low due to non-linear effects; however, it is accurate at lower altitudes. On the other hand, note that since the elevation antenna is located at the GPIP, the nominal touchdown point of the aircraft is past the elevation antenna. Thus, during most of the flare maneuver and touchdown the elevation signal is not available to the aircraft. Hence, before the flare maneuver is started; the filter switches from using the elevation measurement to using the radar altimeter in order to obtain the position of the aircraft. Since at this point the altitude is low, the radar altitude provides reliable data. If a second elevation antenna located further down the runway is present, then this signal could also be used for flare and touchdown.

The values for the standard deviation of the various noises and bias errors in the sensors were chosen to reflect current instrumentation standards [12], [13]; the values are given in Table 1.

B. FILTER EQUATIONS

The measurements obtained from the on-board sensors and the MLS describe the motion of the aircraft and constitute the inputs to the filters. However, to use these measurements as the inputs to a Kalman filter, it is necessary to express them as linear combinations of the state variables. This can be done by preprocessing the measurements which are non-linear functions of the state variables.

Since the attitude of the aircraft, the attitude rates, the barometric and radar altitudes are linear functions of the state variables x and x_ℓ, it is only necessary to pre-process the MLS signals, the accelerometer readings, the baro sink rate and airspeed.

From the expressions for range, azimuth and elevation given in equations (69) , (70), (71) , it is possible to solve for x_o , y_o , z_o .

$$y_o = -R \sin Az \quad , \tag{76}$$

$$x_o = x_e \sin^2 El + \sqrt{x_e^2 \sin^4 El + g^2} \quad , \tag{77}$$

$$z_o = \tan El \sqrt{(x_o - x_e)^2 + (y_o - y_e)^2} \quad , \tag{78}$$

$$g^2 = (R^2 - y_o^2) \cos^2 El - \left((y_o - y_e)^2 + x_e^2 \right) \sin^2 El \quad . \tag{79}$$

Now, x_o , y_o , z_o are linear combinations of the longitudinal and lateral state variables x_ℓ and x, and can be expressed as

$$x'_o = \frac{x_o}{U_o} = -x_{\ell 5} + \frac{x_e}{U_o} + v_{\ell 5} \tag{80}$$

$$y'_o = \frac{y_o}{U_o} = x_6 + v_6 \quad , \tag{81}$$

$$z'_o = \frac{z_o}{U_o} = -x_{\ell 6} + v_{\ell 6} \quad , \tag{82}$$

where $v_{\ell 5}$, $v_{\ell 6}$, and v_6 are additive white noise processes. Thus, these values of x'_o, y'_o and z'_o can be used as inputs to the filter and the expressions (80) , (81) and (82) can be used in the computation of the filter gains.

The specific force measurements obtained from the body-mounted accelerometers can similarly be processed to obtain linear measurements. Using the relationships among the specific force, acceleration, and attitude rates it can be seen that

$$\frac{F_x}{U_o} + L_{BE}(1, 3)\, \bar{g} - \eta_{\ell 2} = \dot{u}'$$
$$= \epsilon_2^T (A_\ell x_\ell + B_\ell u_\ell + D_\ell w_\ell) + b_{ax} + v_{ax} \tag{83}$$

$$\frac{F_y}{U_o} + L_{BE}(2,3)\,\bar{g} - \eta_3 = \frac{\dot{v}}{U_o} + r$$

$$= \epsilon_3^T\,(Ax + Bu + DC_W\,W) + x_5 + b_{ay} + v_{ay} \qquad (84)$$

$$\frac{F_z}{U_o} + L_{BE}(3,3)\,\bar{g} - \eta_{\ell 3} = \frac{\dot{w}}{U_o} - q$$

$$= \epsilon_3^T\,(A_\ell\,x_\ell + B_\ell\,u_\ell + D_\ell\,w_\ell) - x_{\ell 4} + b_{az} + v_{az} \qquad (85)$$

where $\bar{g}$ is $32.2/U_o$, ϵ_i is the ith column of the identity matrix, b_{ax}, b_{ay} and b_{az} are the bias components in the processed versions of the specific forces in the x, y and z directions, respectively, and v_{ax}, v_{ay} and v_{az} are white noise components in the processed measurements. Thus, the left-hand-side of equations (83), (84) and (85) show the processing that needs to be done to the body-mounted accelerometer readings to obtain new pseudo measurements which can be expressed linearly in terms of the longitudinal and lateral state variables; the right-hand-side of the equations show the linear measurement model used.

The barometric sink rate model was obtained directly from the expression given in equation (31) by normalizing the value by U_o and subtracting the predicted value of η_z. The airspeed was linearized using

$$\left[\left(\frac{V_m}{U_o}\right)^2 - (\hat{\beta} + \hat{\beta}_W)^2 - (\hat{\alpha} + \hat{\alpha}_W)^2\right]^{\frac{1}{2}} - 1 = x_{\ell 2} + \epsilon_1^T\,C_{W\ell}\,W_\ell + v\,, \qquad (86)$$

where v is a white noise process.

The processed measurements pertaining to the longitudinal and lateral state variables can be separated and treated with the corresponding dynamical equations. Thus, the roll and yaw angles, the yaw rate and roll rate, the processed MLS y'_o measurement and the processed body-mounted accelerometer F_y measurement were used in connection with the lateral equations of motion, the remaining measurements with the longitudinal equations. Treating each set separately, two filters were developed. The equations of motion were discretized as is shown in section IV, and the steady-state Kalman filter gains were computed. Then, the filtering equations were programmed in a non-linear aircraft dynamics simulation. The filter gains were further adjusted according to the closed loop performance obtained in the simulation runs. The form of the equations for the lateral filter is given below.

$$\nu_k = y_k - C_x \hat{x}_k - C_w \hat{W}_k - C_b \hat{b}_k \quad , \tag{87}$$

$$\hat{x}_{k+1} = \Phi \bar{x}_k + \Gamma u_k + \Gamma_w \bar{W}_k + \Psi \bar{\eta}_k \quad , \tag{88}$$

$$\hat{W}_{k+1} = \Phi_w \bar{W}_k \quad , \tag{89}$$

$$\bar{x}_k = \hat{x}_k + F_x \nu_k \quad , \tag{90}$$

$$\bar{W}_k = \hat{W}_k + F_w \nu_k \quad , \tag{91}$$

$$\hat{b}_{k+1} = \hat{b}_k + F_b \nu_k \quad , \tag{92}$$

where $\hat{x}_k$, $\hat{W}_k$, $\hat{b}_k$ are predicted values and $\bar{x}_k$, $\bar{W}_k$, $\bar{\eta}_k$ are filtered values. A filter of the same form was used for the longitudinal dynamics. Various plots of the filter outputs obtained from the simulation runs are shown in section V.

IV. DEVELOPMENT OF THE CONTROL LAW

The aircraft's motion was modelled by the longitudinal and lateral equations of motion as shown in section II. The model includes the response of the actuator servomechanisms and engine dynamics up to first order, and the effects of wind conditions on the motion of the aircraft. The wind model was developed in section II C using random gust, steady and shear wind components. The filtering equations were described in section III. In this section, these models are used to develop an automatic control law for the final approach till touchdown. The phases of flight considered are the localizer capture and track, steep glideslope capture and track, decrab and flare to touchdown. The lateral and longitudinal control laws are treated separately although some cross-coupling is present; i. e. some longitudinal variables are used for feedback in the control of lateral motion and vice versa. Digital design techniques are used in the development of the control laws by first discretizing the equations of motion into difference equations, and then using a quadratic cost criterion to obtain an optimal control law. The desired flight path is modelled so as to obtain satisfactory performance during the various phases of the final approach.

A. DEVELOPMENT OF THE CONTROL EQUATIONS

Consider the model developed for the lateral motion of the aircraft and the winds which affect this motion as given in equations (56) and (57). Note that the longitudinal equations of motion given in equations (37) and (68) are of the same form as the lateral ones. Thus, the development that follows applies to both models. The lateral equations are given below for convenience.

$$\dot{x} = Ax + Bu + DC_W W + \eta \quad , \tag{56}$$

$$\dot{W} = A_W W + B_W \omega \quad . \tag{57}$$

These differential equations can be expressed equivalently in difference equation form provided that the control u remains constant over the sampling interval; for convenience, we shall further assume that η also remains constant

over the sampling interval, although a more general case can be treated similarly. Hence, if

$$u(t) = u_k \quad , \qquad \eta(t) = \eta_k \quad , \qquad t_k \leq t < t_{k+1} \tag{93}$$

where t_k is the kth sampling instant equal to kT , T being the sampling period, then the differential equations in (56) , (57) can be integrated over the sampling period to obtain a discrete representation [14] , [15], [11].

$$x_{k+1} = \Phi x_k + \Gamma u_k + \Gamma_w W_k + \Psi \eta_k + \omega_{1k} \quad . \tag{94}$$

$$W_{k+1} = \Phi_w W_k + \omega_{2k} \quad , \tag{95}$$

where x_k and W_k are the values of x (t) and W (t) at the sampling instant t_k, respectively, ω_{1k} and ω_{2k} are zero mean white noise sequences with appropriate covariances, and

$$\Phi = e^{AT} = \Phi(T) \ , \ \Phi_w = e^{A_w T} \quad , \tag{96}$$

$$\Psi = \int_0^T \Phi(s) \ ds \quad , \quad \Gamma = \Psi B \quad , \tag{97}$$

$$\Gamma_w = \int_0^T \Phi(T-s) \, DC_w \, \Phi_w(s) \, ds \quad . \tag{98}$$

Thus, the values of the state at the sampling instants can be obtained using the difference equations shown in (94) and (95) .

Depending on the phase of flight, the guidance law will require the aircraft to follow a certain flight path or flight condition. This desired flight path can be described by specifying the values of the state vector x corresponding to this flight condition. Thus, suppose that the vector z (t) describes the desired flight path; then the error in the actual flight path is

$$e(t) = x(t) - z(t) \quad . \tag{99}$$

Since the objective is to follow the desired flight path, z, minimizing a cost function which is quadratic in the error, e, is appropriate; hence,

$$J = \frac{1}{2} E \int_0^{t_f} [e'(t)\, Q\, e(t) + u'(t)\, R\, u(t)]\, dt \quad , \tag{100}$$

where E is the statistical expectation operator. Now, the desired flight path can often be modelled by a differential equation. A model of the following form was used in the development here

$$\dot{z} = A_z\, z + \zeta_z \quad , \tag{101}$$

$$\dot{\zeta} = \xi_z \quad , \tag{102}$$

where ξ_z is assumed to a gaussian white noise process. Thus, the desired flight path is modelled as a random process; i.e., it is modelled as belonging to a family of trajectories which has given statistical properties. Inherent in this formulation is the fact that the desired flight path is not necessarily known a priori; i.e., the future values of z are not necessarily known at the outset; hence, future values of the desired flight path are not needed to compute the current value of the control. Future values of the z would be necessary if it were modelled as a deterministic flight path [16]. Using this model for z, the equations of motion in (56) and (57), the cost function, J, can be expressed in an equivalent discrete form [15], [11].

$$J_1 = \frac{1}{2} E \sum_{k=0}^{N} e'_k \hat{Q} e_k + u'_k \hat{R} u_k + 2\,(e'_k \hat{N} d_k + e'_k \hat{M} u_k + d'_k \hat{S} u_k) \tag{103}$$

$$\hat{Q} = \int_0^T \Phi'(s)\, Q\, \Phi(s)\, ds \quad , \tag{104}$$

$$\hat{R} = \int_0^T \Gamma'(s)\, Q\, \Gamma(s)\, ds + RT \quad , \tag{105}$$

$$\hat{M} = \int_0^T \Phi'(s)\, Q\, \Gamma(s)\, ds \quad , \tag{106}$$

$$\hat{N} = \int_0^T \Phi'(s)\, Q\, \Gamma_d(s)\, ds \quad , \tag{107}$$

$$\hat{S} = \int_0^T \Gamma'_d(s)\, Q\, \Gamma(s)\, ds \quad . \tag{108}$$

The continuous and discrete cost functions J and J_1 differ by a constant which does not depend on u_k ; hence, the same control minimizes both cost functions. The

optimal control sequence which minimizes the cost function J given in (100) with the constraint that the control remain constant over the sampling period can be shown to be of the form [11] , [17].

$$u_k = -H_e (\bar{x}_k - z_k) - H_w \bar{W}_k - H_z Z_k - H_\zeta (\zeta_{zk} - \bar{\eta}_k) \quad , \tag{109}$$

where $\bar{x}_k$, $\bar{W}_k$ and $\bar{\eta}_k$ are filtered least mean square estimates.

B. MODELLING OF THE DESIRED FLIGHT PATH

The feedback control given in the last section requires that the model for the desired flight path, z, given in (101) and (102) be specified, since the values of z and ζ_z enter directly into the computation of the control commands. Note, however, that the matrix A_z in the model is also used in the computation of the feedback gains, and thus must also be specified.

The phases of the final approach considered here are the localizer capture, localizer track, glideslope capture and track, decrab and flare. The aircraft must perform these maneuvers in a constant airspeed, 3D mode. Thus, it is assumed that the aircraft is approaching the runway in level flight at a specified heading which intersects the runway centerline at a specified point. At some point on this flight path, the localizer capture mode is engaged, and the automatic control law controls the aircraft through the various phases of the final approach till touchdown.

The localizer capture engage logic was developed so that the initial rolling tendency of the aircraft is to bank away from runway centerline, thus avoiding overshoot tendencies. Now, let $\bar{\psi}$ be the yaw angle estimate and $\bar{y}'$ the estimate of the normalized distance of the aircraft from runway centerline. Now, assuming that the remaining variables in equation (109) are small, the aileron command, δA, will be given by

$$\delta A = -H_e (1, 2) \bar{\psi} - H_e (1, 6) \bar{y}' \quad . \tag{110}$$

Thus, localizer capture should be engaged when the aircraft crosses the curve obtained by setting δA equal to zero. Further observation of the situation leads to the following criterion.

$$\left| \bar{y} \right| \leq U_o \left| \frac{H_e(1,2)}{H_e(1,6)} \bar{\psi} \right| , \tag{111}$$

where U_o is the inertial speed of the aircraft, and $\bar{y}$ is the distance from runway centerline. Thus, localizer capture is engaged when the criterion in (111) is met. It should be noted that this criterion is useful as long as $\bar{y}$ has a small error as would be the case when the MLS signal is valid; if the position estimate has large errors, capture could be initiated too early or too late to reduce overshoots.

The desired flight path for the lateral motion of the aircraft was chosen to be the runway centerline, with the desired cross-runway velocity being zero. Under no wind conditions, the desired yaw and roll angles as well as their rates of change are zero; however, if a cross wind is present the aircraft should crab into the wind and then decrab before landing while keeping a small aerodynamic sideslip angle throughout the flight. It is also desired that any overshoot or undershoot during localizer capture be as small as consistent with the other requirements. The desired flight path in equations (101), (102) was modelled using

$$Az = A \quad , \quad \zeta_z = \dot{z} - Az \quad , \tag{112}$$

for the lateral dynamics. The discrete form was used to update the desired flight path.

$$z_{k+1} = \Phi \, z_k + \Psi \, \zeta_{zk} \quad . \tag{113}$$

In order to have the aircraft crab into the wind rather than use a bank angle, the yaw angle weight was set to zero and the desired inertial sideslip angle was set equal to the negative value of the estimate of the sideslip angle due to steady cross-winds.

$$z_{k3} = - \bar{\beta}_{ws} \quad . \tag{114}$$

To reduce overshoots, the closed loop damping on lateral offset was obtained by using a non-zero weight on the cross-runway velocity. Decrab was obtained by setting the desired roll rate to be proportional to the deviation in the yaw angle from the runway heading, and, simultaneously, setting the desired yaw rate proportional to the yaw angle deviation, when the aircraft crosses the decrab altitude.

An exponential "easy-on" was used to introduce the decrab commands in order to avoid sudden changes in the commands and the ensuing transient response.

The desired flight path for the longitudinal variables, z_ℓ, was specified in a similar manner. To obtain a constant airspeed of U_0, the normalized desired inertial speed along the stability x-axis was set equal to the difference between the normalized desired airspeed and the normalized wind velocity estimate along the stability x-axis.

$$z_{\ell 2} = 1 - \epsilon_1' \; C_{w\ell} \; \bar{W}_\ell \quad , \tag{115}$$

$$\zeta_{z\ell 2} = -\epsilon_1' \; C_{\dot{w}\ell} \; A_{w\ell} \; \bar{W}_\ell \quad . \tag{116}$$

To follow a glideslope of angle γ_0, the inertial velocity must point along the glideslope; the desired angle of attack of the inertial velocity was set so as to obtain this proportion between the x_e and z_e components of the inertial velocity.

$$z_{\ell 3} = -\Big((\bar{L}_{31} + \tan\gamma_0 \; \bar{L}_{11}) \; (1 + z_2) + \big(\bar{L}_{32} + \tan\gamma_0 \; \bar{L}_{12} \big) \bar{\beta} \Big) / \big(\bar{L}_{33} + \tan\gamma_0 \; \bar{L}_{13} \big) \; , \tag{117}$$

where $\bar{L}_{ij}$ is the estimate of L_{ES} (i, j) and $\bar{\beta}$ is the estimate of the inertial sideslip angle.

To obtain a 3D control law the longitudinal model developed in section II was slightly modified; however, the filter development is based on the unmodified model. To make the control law independent of the x position of the aircraft, this variable was excluded from the control model; thus, the number of state variables were reduced by one. On the other hand, the altitude variable ($x_{\ell 6}$) was modified to represent the altitude error from the glideslope. This error was defined as the difference between the aircraft's actual altitude and the altitude of the point on the glideslope corresponding to the aircraft's actual x position; i. e.,

$$x_{\ell 6} = Z'_e + \tan\gamma_0 \; X'_e \quad , \tag{118}$$

where X'_e and Z'_e are the x and z components of the aircraft's position in the earth-fixed coordinate frame normalized by U_0. After some manipulation, a differential

equation for $x_{\ell 6}$ in terms of the other state variables can be obtained.

$$\dot{x}_{\ell 6} = -x_{\ell 1} + \sec\gamma_0 \; x_{\ell 3} + \eta_{\ell 6}$$

$$\eta_{\ell 6} = (L_{61} + \tan\gamma_0 L_{11}) (1 + x_{\ell 2}) + (L_{63} + \tan\gamma_0 L_{13}) x_{\ell 3} + (L_{62} + \tan\gamma_0 L_{12}) \beta$$

$$+ x_{\ell 1} - \sec\gamma_0 \; x_{\ell 3} \quad , \tag{119}$$

where L_{ij} is L_{ES} (i, j) , and β is the inertial sideslip angle, x_3 , from the lateral model. The model $A_{z\ell}$ used was the same as the one given in [11] with the change that $z_{\ell 5}$ was omitted and $z_{\ell 6}$ was given by

$$\dot{z}_{\ell 6} = -z_{\ell 1} + \sec\gamma_0 \; z_{\ell 3} + \zeta_{z\ell 6} \quad . \tag{120}$$

To obtain $\zeta_{z\ell 6}$, $\dot{z}_{\ell 6}$ was first computed by

$$\dot{z}_{\ell 6} = \dot{Z}'_{ed} + \tan\gamma_0 \; \bar{\dot{X}}'_e \quad , \tag{121}$$

where $\dot{Z}'_{ed}$ is the desired normalized sink rate, and $\bar{\dot{X}}'_e$ is the estimate of the aircraft's inertial velocity along x_e. Thus, $\dot{z}_{\ell 6}$ is obtained; then $\zeta_{z\ell 6}$ is computed by solving equation (120) .

The control feedback gains for the longitudinal control law were computed using the modified model for the motion of the aircraft. Various changes in the gain values were made to improve performance as obtained from simulation runs.

V. RESULTS

The performance of the automatic landing system described in the preceding sections was evaluated using a non-linear digital simulation of a Boeing 737 aircraft. Since the automatic landing control law was developed using linear methods of modern control theory and was tested with a linear simulation of the aircraft using perturbation equations, evaluating its performance with a more accurate, six-degree-of-freedom, non-linear simulation of the aircraft was considered to be a realistic approach to its performance evaluation. The sensor models used in this simulation were also more accurate in their generation of error signals and noisy readings.

The flight paths considered in the evaluation consist of steep final approach paths starting at localizer capture and ending at touchdown. Thus, at the beginning of the simulation, the aircraft is assumed to be in level flight, approaching the runway at approximately 61.73 m/sec (120 knots) on a straight line which intercepts the runway centerline at a specified track angle and a corresponding yaw angle. When the criterion given by (111) is met, the localizer capture mode is engaged and the control law starts to align the aircraft with the runway. Similarly, when the glideslope capture criterion is met, the aircraft starts the glideslope capture maneuver, which brings the aircraft to a steep glideslope (6°) by pitching down and increasing the sink rate to its appropriate value depending on wind conditions. Since the control law tries to maintain a constant airspeed, in a head wind condition, the ground speed will be lower, and to stay on the glideslope, the aircraft will have a lower sink rate; in a tail wind condition, the situation would be reversed resulting in a higher sink rate.

By appropriate choice of the initial altitude, the localizer and glideslope capture modes can be initiated at the same time. In this case, both capture maneuvers occur simultaneously; and the aircraft follows a curved path in the horizontal plane while also following a curved path in the vertical plane. Thus, the aircraft banks away from the runway to reduce its cross-runway velocity while it is pitching down to increase its sink rate. This simultaneous capture of localizer and glideslope is

desirable as it reduces the amount of time (and space or distance) used in the capture maneuvers. It allows aircraft to perform the capture maneuver closer to the runway, thus using less space on runway centerline which now becomes available for other aircraft. Thus, the aircraft can perform close-in simultaneous localizer and glideslope captures. The simulation runs made for the evaluation of the control law were chosen so as to perform simultaneous captures.

Another factor which affects close-in captures is the amount of time it takes for the aircraft to arrive at a stable condition on the glideslope and localizer, i.e. the capture settling time. Thus, if the settling time is small the aircraft is ready to start the subsequent maneuvers, in this case decrab and flare.

This would allow the aircraft to start the capture maneuvers closer to the runway. Thus, in the development of the control law, an effort was made to complete the localizer and glideslope capture in a short period of time by avoiding large overshoots and undershoots, and large time constants for the closed-loop system. As can be seen from the plots of the various parameters obtained from the simulation runs, it takes approximately 40 seconds for the aircraft to complete the simultaneous localizer and glideslope captures and settle in a steady flight condition on the glideslope, starting from level flight with localizer intercept angles of up to 40°.

In cases where the wind velocity has a cross-wind component, the lateral control law automatically crabs the aircraft into the wind, while remaining on runway centerline; thus, the aerodynamic sideslip angle is kept small. This is achieved by estimating the magnitude of the cross-wind component and feeding this information back through the control commands. The various plots obtained from simulation runs where a cross-wind is present show that the control law achieves the correct crab angle for the various wind conditions considered as can be seen by checking the yaw angle of the aircraft relative to runway centerline and its offset from runway centerline. Also, note that no excessive overshoots are present in localizer capture in these cases, irrespective of the direction of the cross-wind. This performance is also due to the estimation and feedback of the wind velocity.

When the aircraft has a crab angle due to cross-winds, the decrab mode is engaged when the estimated altitude reaches a specified altitude. This decrab altitude is currently set at 76.2 m since the aircraft is on a steep glideslope and its sink rate is higher than the conventional 2.5° - 3° glideslopes. The decrab law is designed to align the aircraft's x body axis with the runway centerline; i.e. it reduces the crab angle by rolling into the wind while the yaw angle is reduced to zero. This is achieved by commanding the aircraft to roll into the appropriate side until the yaw angle reaches zero. A yaw rate command proportional to the yaw angle is also used to aid in the maneuver. The simulation runs conducted show that the aircraft reduces its yaw angle and rolls into the wind while remaining on runway centerline when the decrab mode is engaged; the results under cross-winds accompanied by gusts also appears satisfactory in the simulation runs made.

As in the case of the decrab altitude, flare is initiated at a higher altitude than it would be for shallower glideslope angles due to the fact that the sink rate is higher with steep glideslopes. Thus, the flare mode is engaged when the aircraft's estimated altitude reaches 50.50 m. Since the sink rate is higher on a steep glideslope and flare is a flight critical phase final approach, initiating flare at a higher altitude has the advantage of lowering the sink rate to more conventional levels at a higher altitude. This provides the advantages of a slower and more stable flare maneuver, and leaves more time and altitude for the pilot to monitor the progress of the maneuver with ease. In this mode, the aircraft follows a flare path with a specified vertical profile until touchdown. The flare path is generated on line with the independent variable being the distance to the GPIP. The simulation runs show that the flare law achieves satisfactory landings under the various wind conditions considered.

The digital nonlinear simulation ALERT was used for the aircraft dynamics of the B-737 and the various sensor dynamics and errors. The aircraft dynamics model in ALERT uses the six-degree-of-freedom nonlinear equations of motion. The aerodynamic forces are generated using the stability derivatives of the B-737 aircraft for an airspeed of 61.73 m/sec (120 knots). A detailed description of the

simulation can be found in [18] . The basic update rate for the simulation of the aircraft dynamics was 20 samples per second, corresponding to a period of 50 msec.. The digital control law operates at a sampling rate of 10 Hz, or twice as slow as the basic simulation update rate. Thus, the sensor measurements were sampled every 100 msec. although they were available every 50 msec. in the simulation.

The MLS signals of azimuth, elevation and range, were simulated by corrupting the true values by an error signal. The error signal contained noise and bias to model the effects of calibration errors and misalignments in the installment of the antennae. The jitter that has been added to the MLS signals to avoid interference was also modelled and simulated in the error signal. The body-mounted accelerometers were modelled so as to include the effects of misalignment relative to the aircraft's body axes, errors in scaling, bias and noise. Thus, the true values of the specific force components along the body axes are rotated to obtain the readings of the misaligned specific force components, then scaling error effects are introduced before the bias and noise are added. The attitude rate gyros and airspeed indicator were modelled as being corrupted by noise, whereas the attitude gyro, barometric altitude and sink rate and radar altimeter measurements contained bias errors and noise; the noises in airspeed and barometric sink rate were introduced as multiplicative noise. The values for the standard deviation of the noises and other errors reflect current instrumentation standards [12] , [13] . Table 1 shows the values of the various parameters used in the error models of the sensors.

Numerous simulation runs were conducted using the ALERT simulation of the aircraft and navigation aids in partial evaluation of the overall performance of the control law developed. Various parameters describing the response of the closed loop system (aircraft dynamics, sensors and control law) were plotted. Figures 5 - 20 show the plots of these parameters for some of the simulation runs conducted. These simulations show the response of the aircraft under steady winds of 5.14 m/sec (10 knot) velocity from various directions: head winds, tail winds,

cross winds and other combinations, turbulence of various intensities with and without steady winds, and under wind shear conditions. For the purposes of this investigation, wind gusts with a standard deviation of .61 m/sec in the forward and lateral directions (x and y body axes) and .30 m/sec in the vertical direction were denoted as average turbulence levels; doubling the standard deviation of the wind gust velocities in all three directions was accepted as a high turbulence level. The wind shear conditions were simulated starting at an altitude of 60.96 m and ending at touchdown. From 60.96 m to 30.48 m of altitude the steady wind is decreased linearly at a rate of 2.06 m/sec (4 knots) per 30.48 m (100 feet); from 30.48 m to touchdown the steady wind changes at a rate of 4.12 m/sec (8 knots) per 30.48 m. Thus, the steady wind component changes 6.17 m/sec (12 knots) in 60.96 m preceeding touchdown with the rate of change increasing as the aircraft gets closer to touchdown and during flare.

Various of the simulation runs made under combinations of steady winds, turbulence levels, turbulence patterns or histories and wind shear conditions are shown in Figures 5 - 20 . Localizer captures with differing intercept angles were also simulated to examine the capture response under differing initial conditions. Simulations of the final approach with nominal airspeeds of 61.73 and 64.30 m/sec were made, with the majority of the runs being at the 61.73 m/sec design airspeed. On various occasions, the initial conditions were offset from the desired, nominal or trim values; the initial values of the filter estimates were also intentionally set to incorrect values to assess their effects on performance. Various other parameters were also changed during the evaluation to check their sensitivity and to improve the response.

From the simulation runs made, it is seen that the overall performance of the control law during the final approach, starting from localizer and glideslope capture to touchdown, is satisfactory under the various wind conditions considered. The simultaneous localizer and glideslope capture maneuvers are performed and completed in a short period of time and without excessive overshoots in the presence of head winds, cross winds and turbulence as well as under no wind cases. When the aircraft is approaching the runway centerline at a 30° track angle localizer capture is initiated at 361 m offset from centerline; observation of the plots for this initial condition (as well as others) shows that localizer capture is completed

in less than 40 seconds, so that for all practical purposes the aircraft has settled on runway centerline. It can further be seen that the lateral overshoot in these cases is small, sometimes barely noticeable, and rarely exceeding 7.6 m at its peak. The lack of an appreciable overshoot in lateral offset can be traced to the use of wind velocity estimates in the feedback control; when the initial cross wind estimate (at capture initiation) has a 5.14 m/sec error, larger overshoots approaching 15 m are obtained before the error in the estimate is reduced to lower levels. These situations can be avoided by running the filter open loop before the control law is engaged. On the other hand, a more basic approach would be to use a sensor measuring the aerodynamic sideslip angle (such as a β - vane or other sensor) to reduce the time constant related to the cross-wind estimate. This would reduce the error in the wind estimate in a shorter period of time and reduce any overshoot as well as aid in gust alleviation and wind shear accomodation.

Similar remarks can be made about the glideslope capture which is performed at the same time as localizer capture. From the various plots, it can be seen that the aircraft settles on the glideslope in about 20 seconds as the aircraft is more responsive vertically and the offsets involved are smaller. It may be noted that, under no wind conditions, the aircraft has a vertical offset which gets smaller as it gets closer to the runway. This is due to the bias or misalignment simulated in the MLS elevation signal which is not accounted for by the filter. A similar offset with a decreasing trend can be seen in the lateral direction due to the bias in the MLS azimuth signal simulation. The effects of these offsets are small, predictable, and are considered of minor significance relative to other offsets.

The overall performance during flare and touchdown under various wind conditions is shown in Figures 5 - 20. The sink rate which holds a constant level on the glideslope gradually decreases to a smaller value and tries to maintain this lower rate until touchdown. The desired sink rate at touchdown was chosen to be .64 m/sec (2.1 ft/sec) at 61.73 m/sec. This constant sink rate command until touchdown was used to reduce the touchdown dispersion when wind conditions tend to make the aircraft float past its nominal touchdown point. The plots of the aircraft's sink rate under various wind conditions show a satisfactory response during the various phases

of flight and flare. In the simulation runs made, the touchdown sink rate has a mean or average value of .66 m/sec and a standard deviation of .26 m/sec. The average value of the touchdown points was 416 m from the GPIP with a standard deviation of 34.5 m. Table 2 shows the touchdown sink rate and the deviation in the touchdown point for some of the simulation runs made under differing wind conditions. It should also be noted that the other parameters relevant to the touchdown condition such as pitch attitude, yaw angle, offset from runway centerline, etc. also had satisfactory values as can be seen from Figures 5 - 20.

In comparison to simulations of the autoland control law currently used with the third order complementary filter or the time varying Kalman filter [18], [19], [20], the digital control law described above has smaller overshoot peaks and requires less time to settle to a steady condition during the localizer and glideslope capture maneuvers. It should also be noted that the latter law performs the localizer and glideslope captures simultaneously and follows a steep glideslope. The latter law computes estimates of the wind velocity components and uses these estimates in the feedback control commands whereas the current autoland law uses a wind shear detector. A difference in the design approach is due to the fact that the current autoland control law was developed as a continuous or analog system and was implemented on a digital computer using a 20 Hz sampling rate, whereas the latter control law was developed as a digital or discrete system based on a 10 Hz sampling rate using modern digital control techniques.

In conclusion, the digital automatic landing guidance and control law, as seen from the simulation evaluation described above, has satisfactory performance in the final approach to landing phases of flight.

VI. SUMMARY

A digital guidance and control law for a steep final approach was developed using modern digital control techniques for operation in a 3D constant airspeed mode. To take advantage of the high precision MLS guidance information, a constant gain digital Kalman filter which combines the MLS information with various on-board sensor outputs was developed to obtain accurate estimates of the aircraft's position, velocity, attitude and the wind velocity components. The wind velocity estimates are used in the feedback control law along with the other dynamical variables for gust alleviation and wind shear detection and control. The control law considers simultaneous localizer and glideslope capture, localizer and glideslope tracking, crab and decrab, and flare to touchdown. The digital filter and control law were simulated on a digital computer with a non-linear simulation of the B-737 aircraft, on-board sensors and the Microwave Landing System. Simulation runs made under varying wind conditions show satisfactory performance of the automatic control system throughout the final approach.

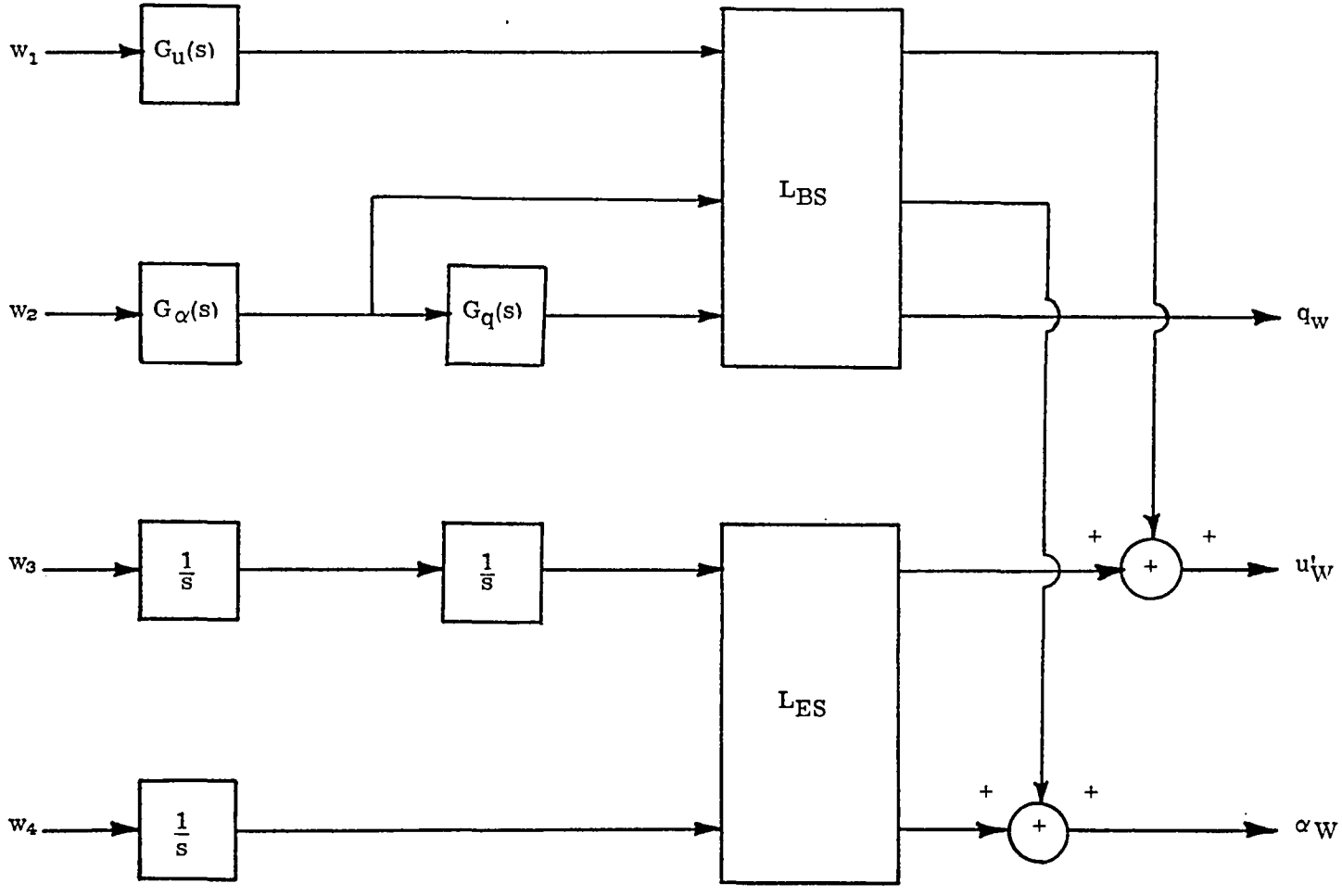

Figure 1 Longitudinal Wind Model

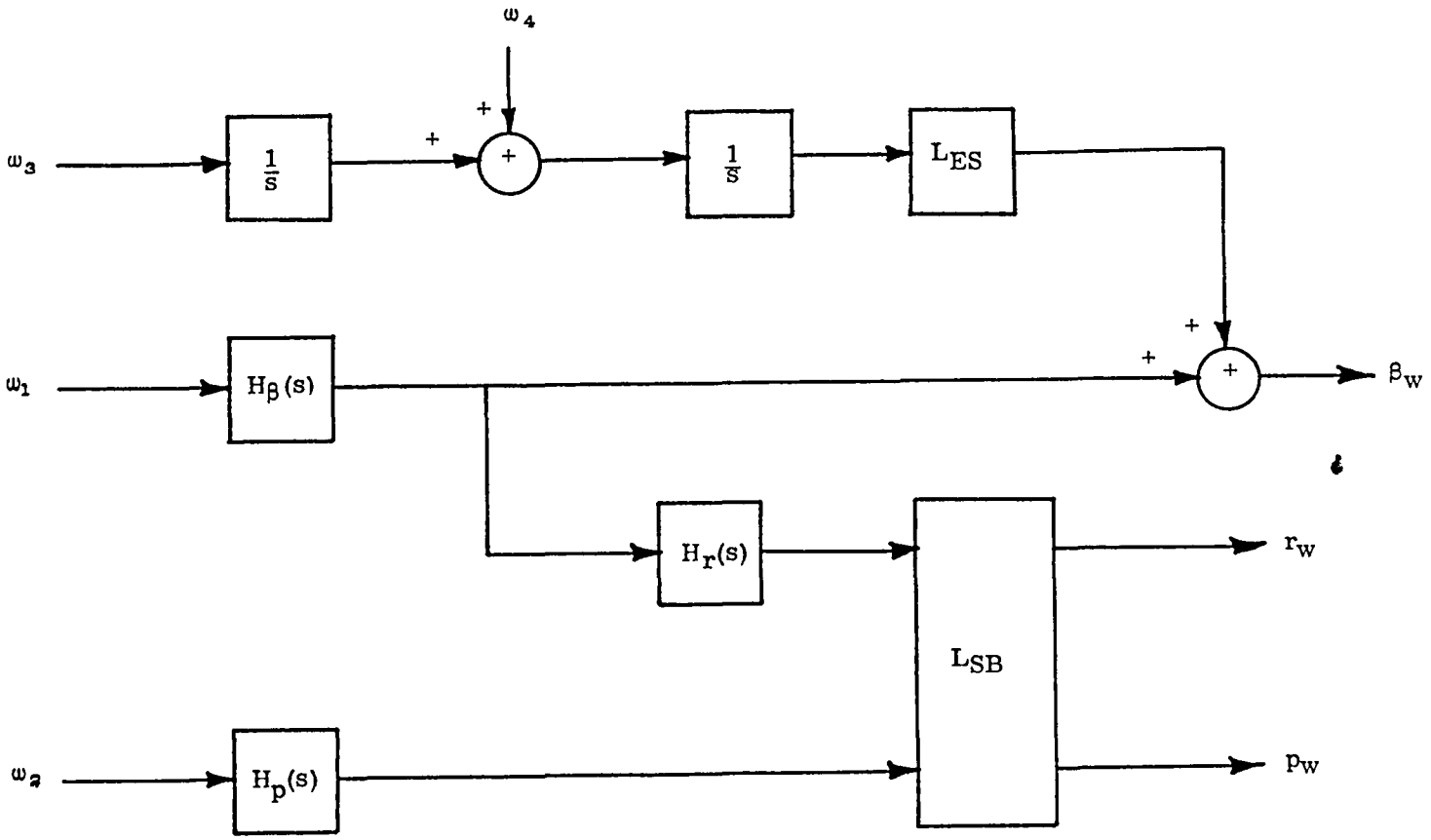

Figure 2 Lateral Wind Model

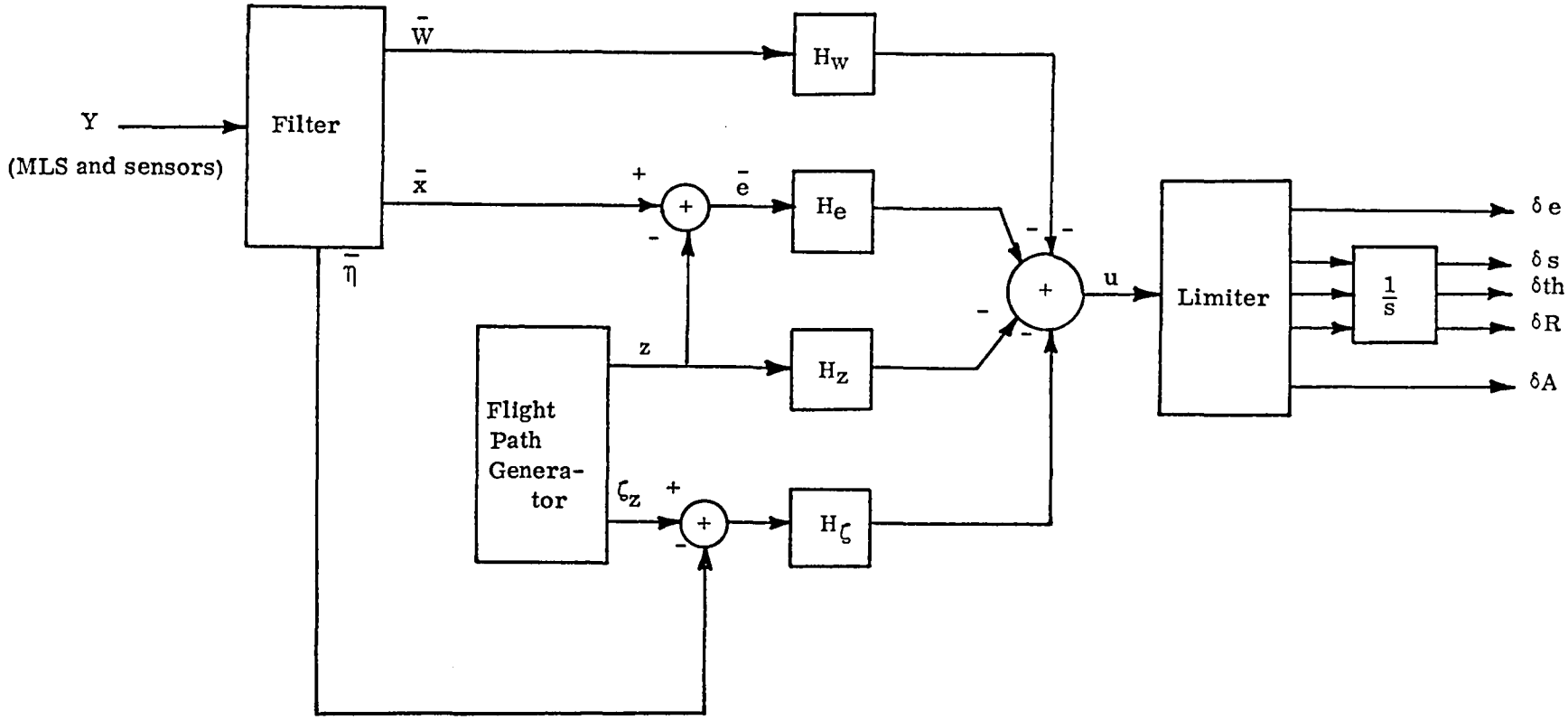

Figure 3 Block Diagram of Feedback Loop

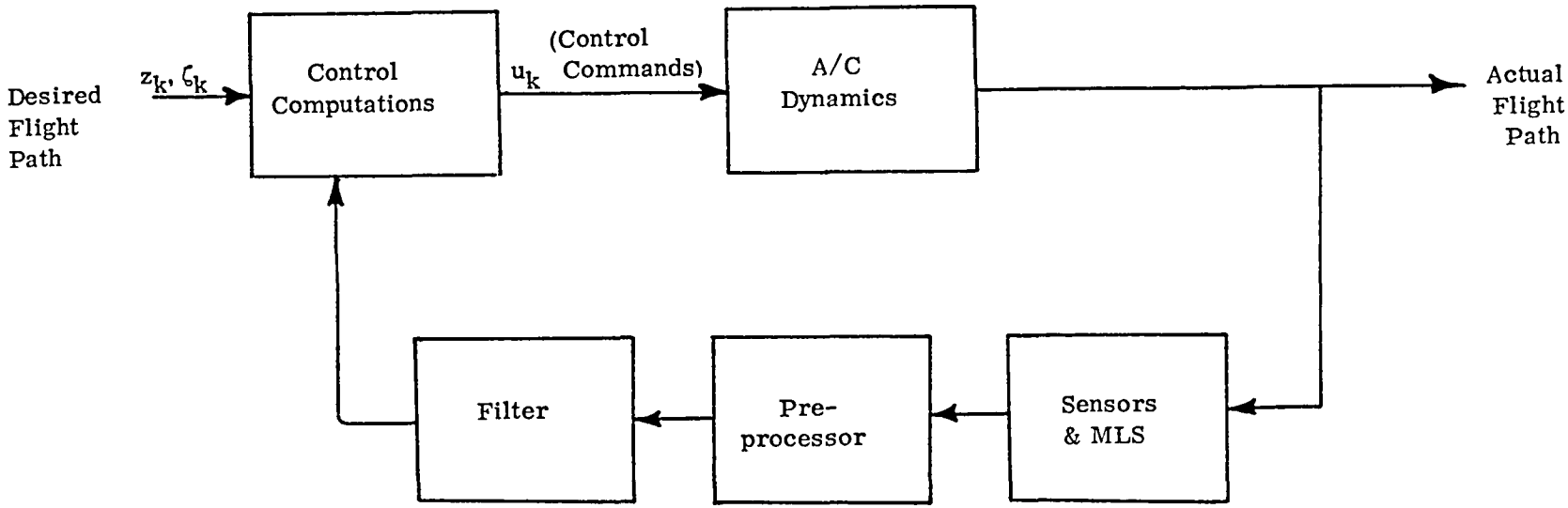

Figure 4 Functional Block Diagram of Closed Loop System

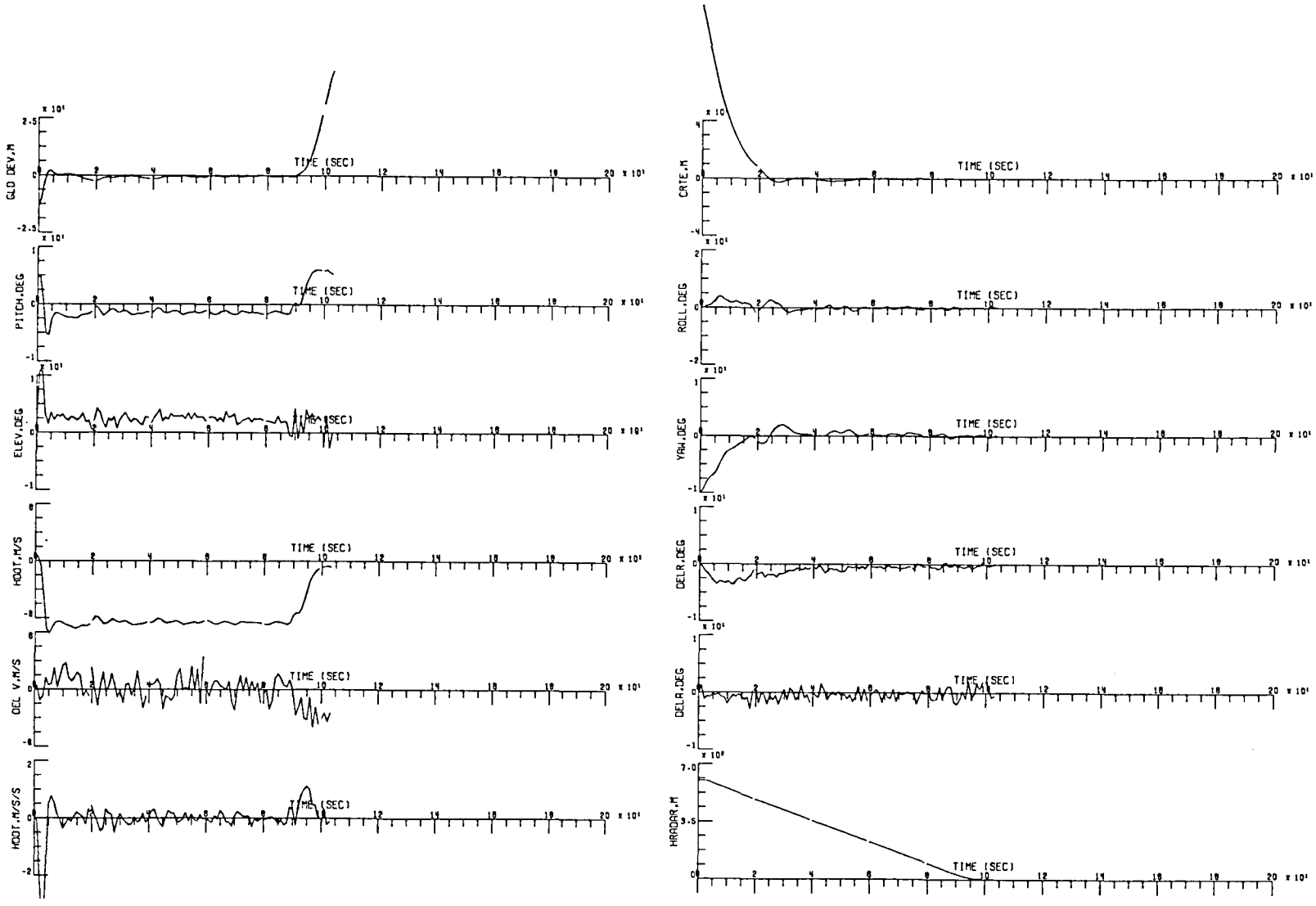

Figure 5 Final Approach Simulation: 10° localizer intercept

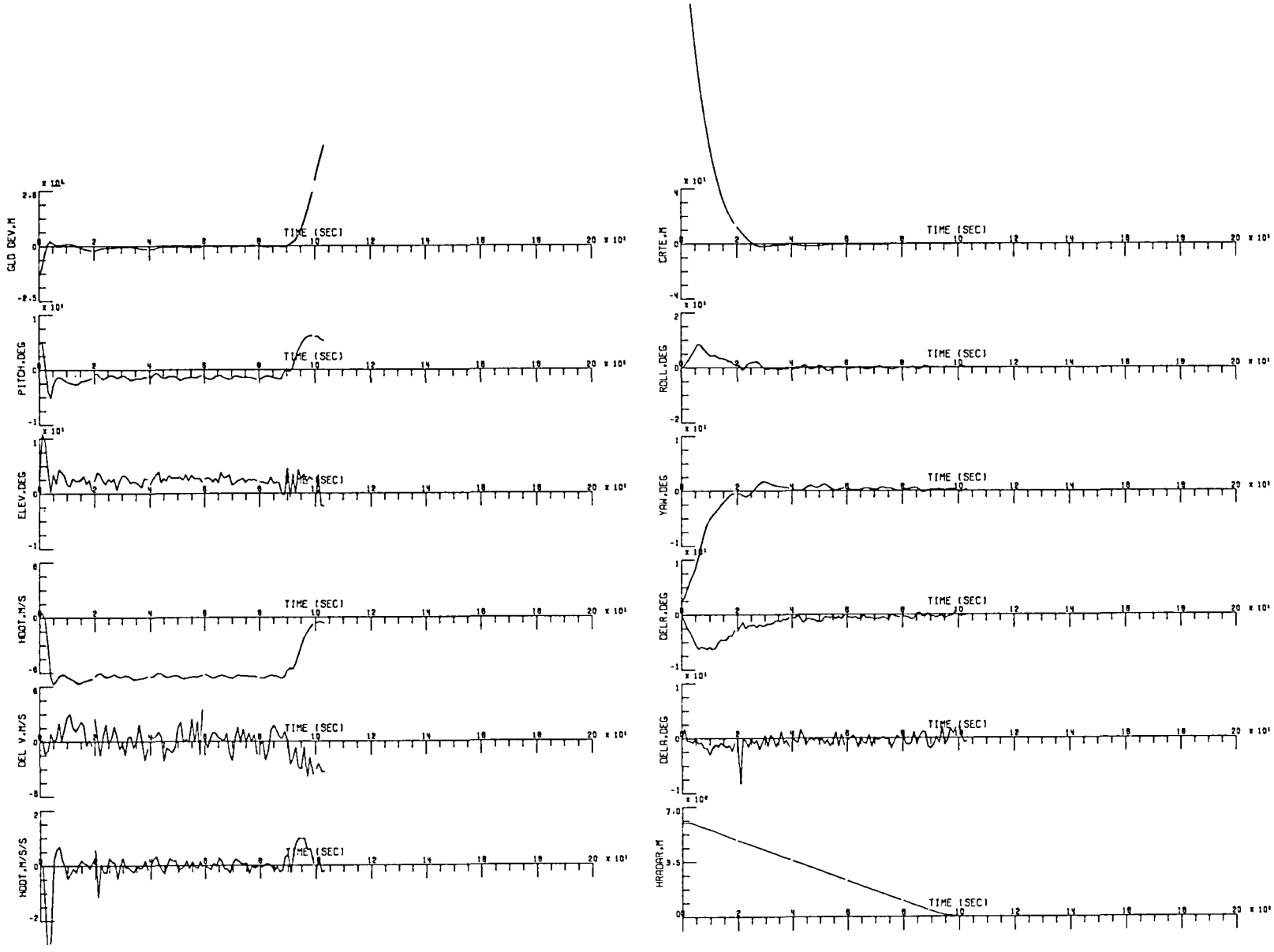

Figure 6 Final Approach Simulation: 20° localizer intercept

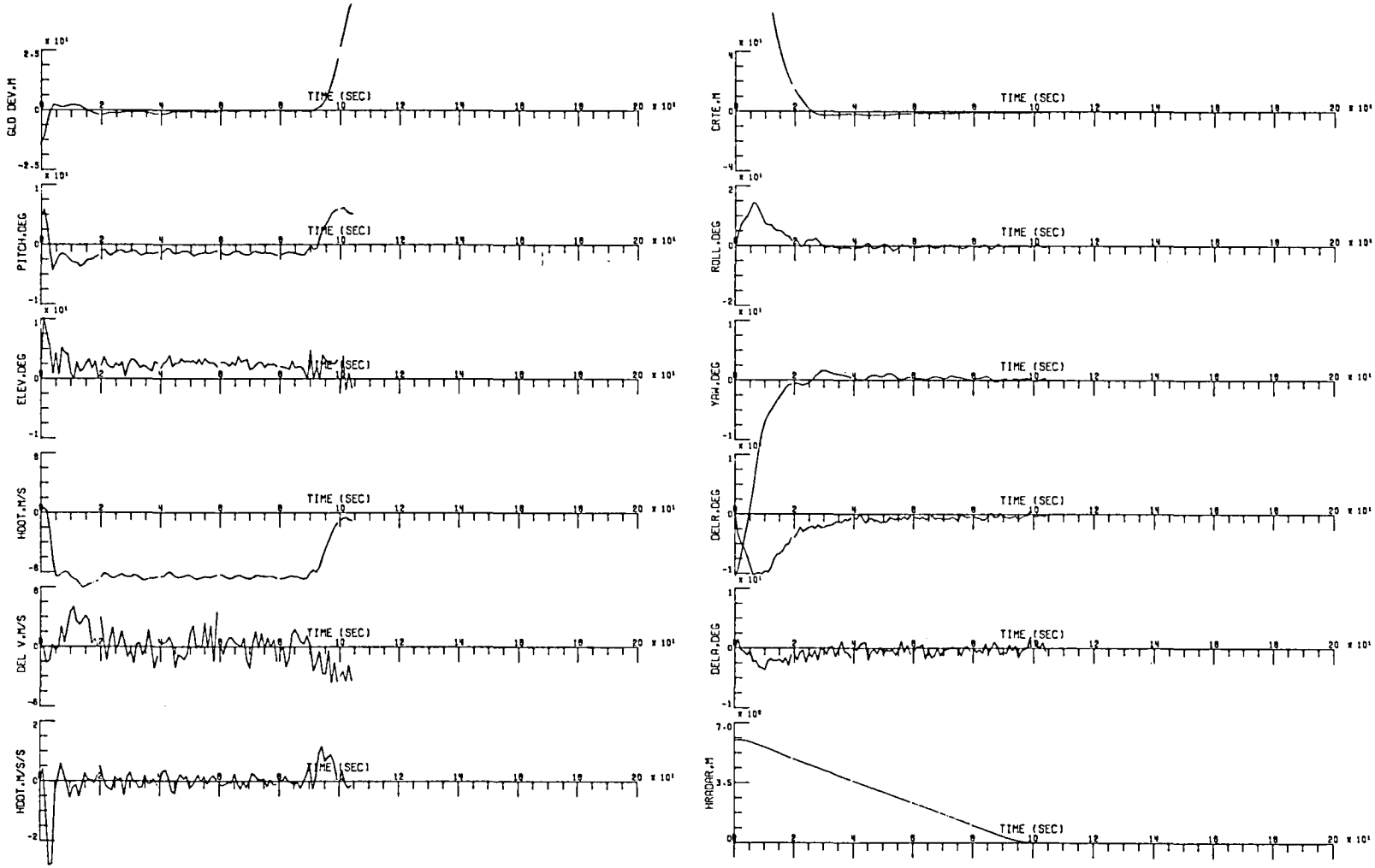

Figure 7 Final Approach Simulation: 30° localizer intercept

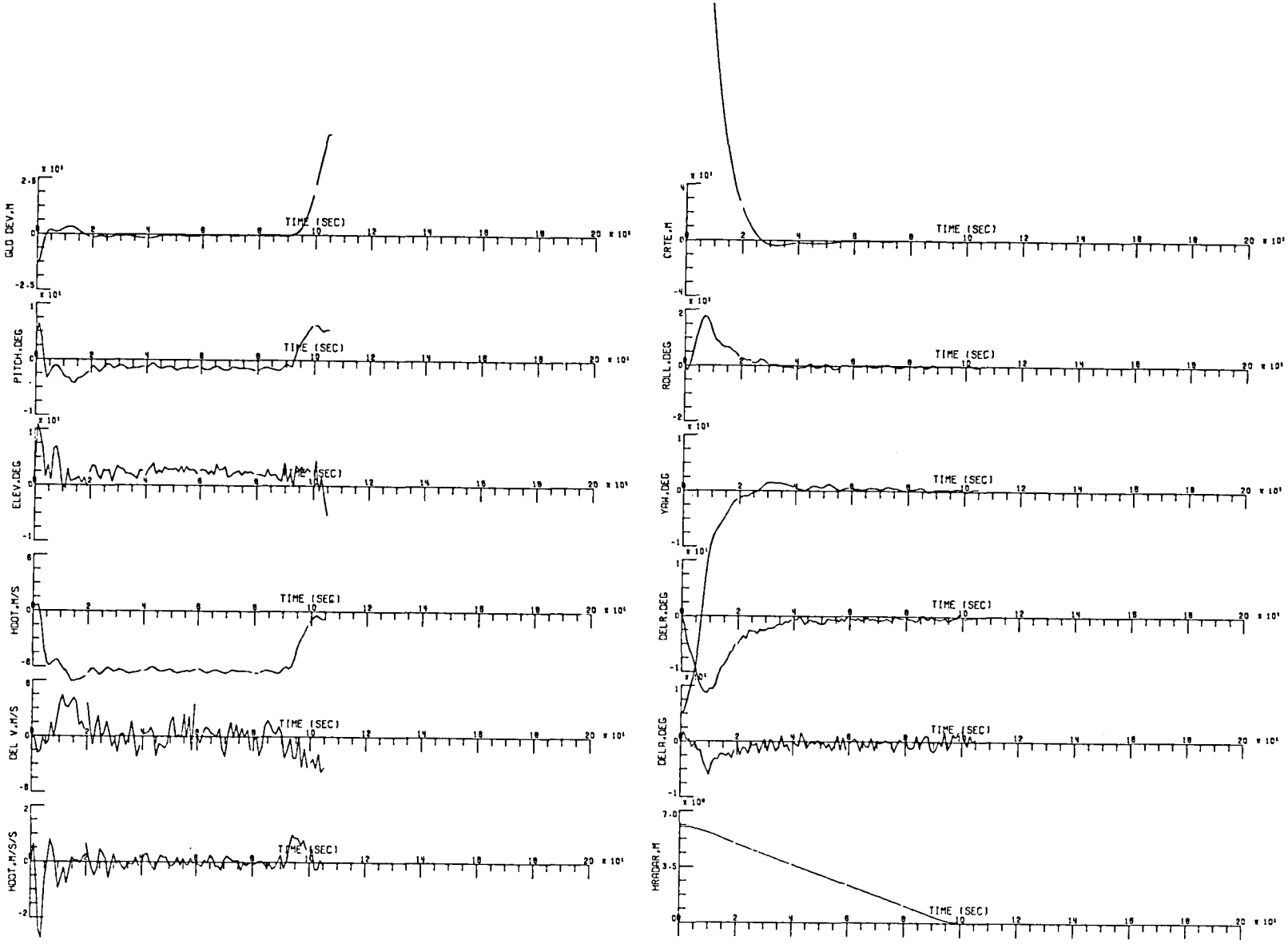

Figure 8 Final Approach Simulation: 40° localizer intercept

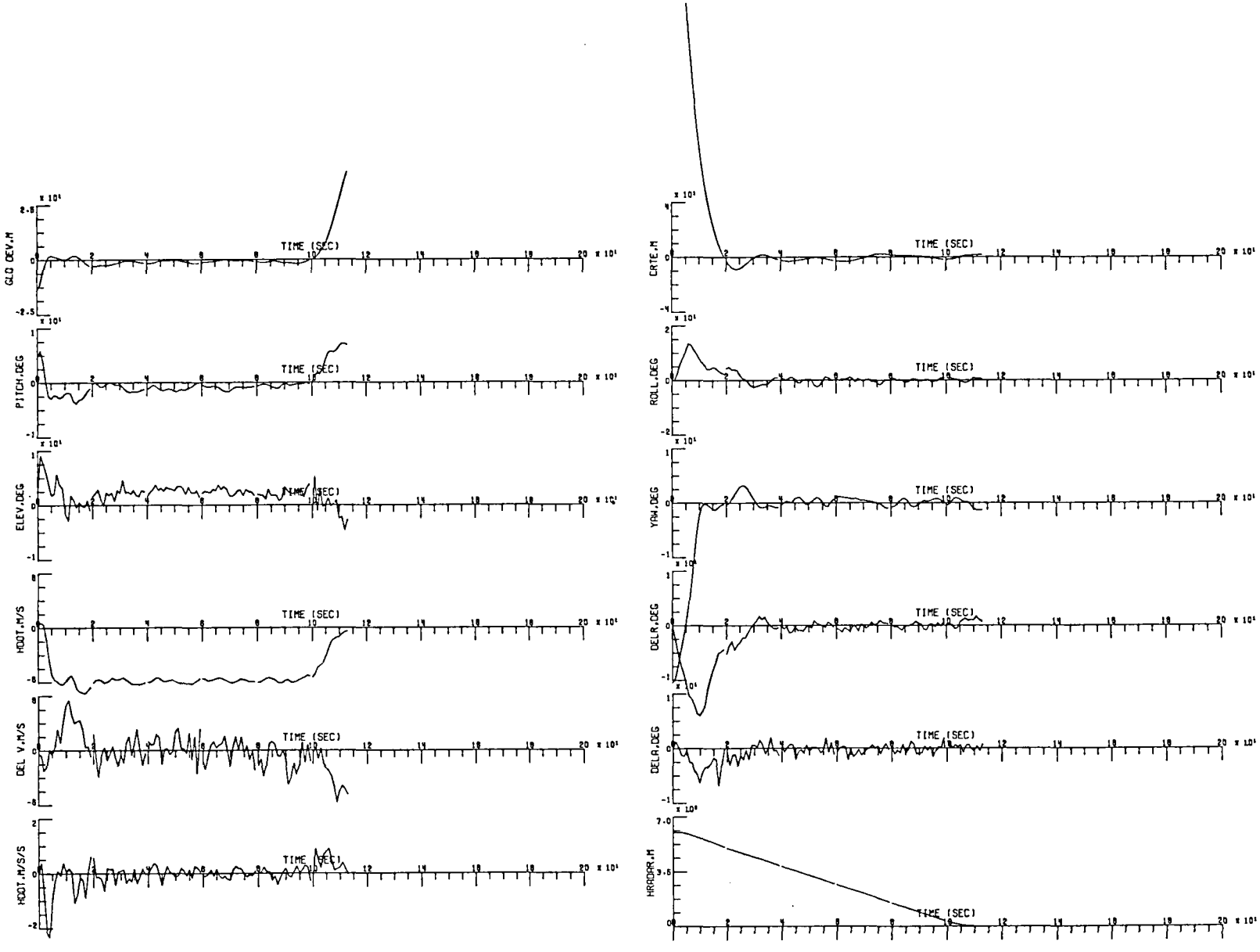

Figure 9 Final Approach Simulation: head wind, average turbulence

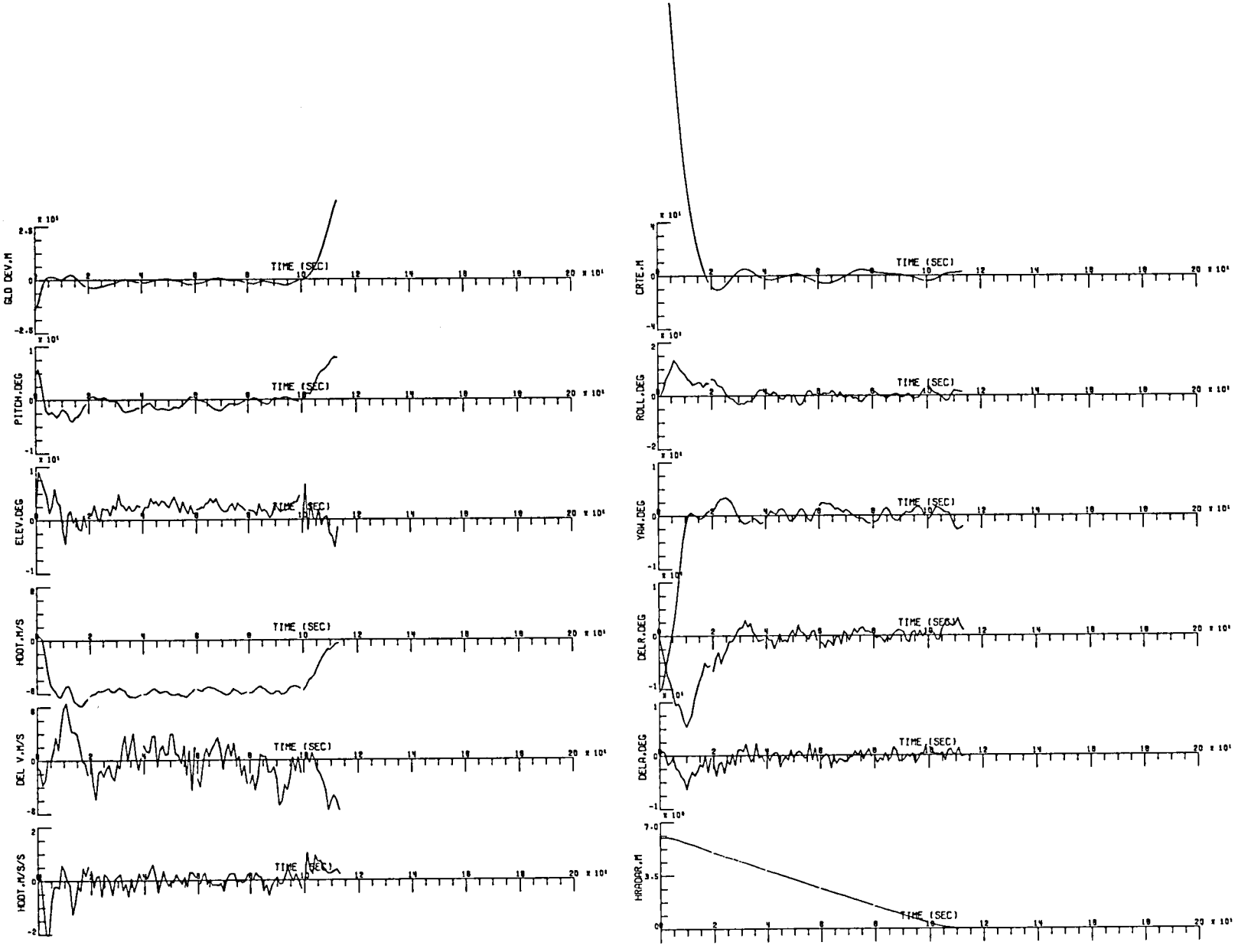

Figure 10 Final Approach Simulation: head wind, high turbulence

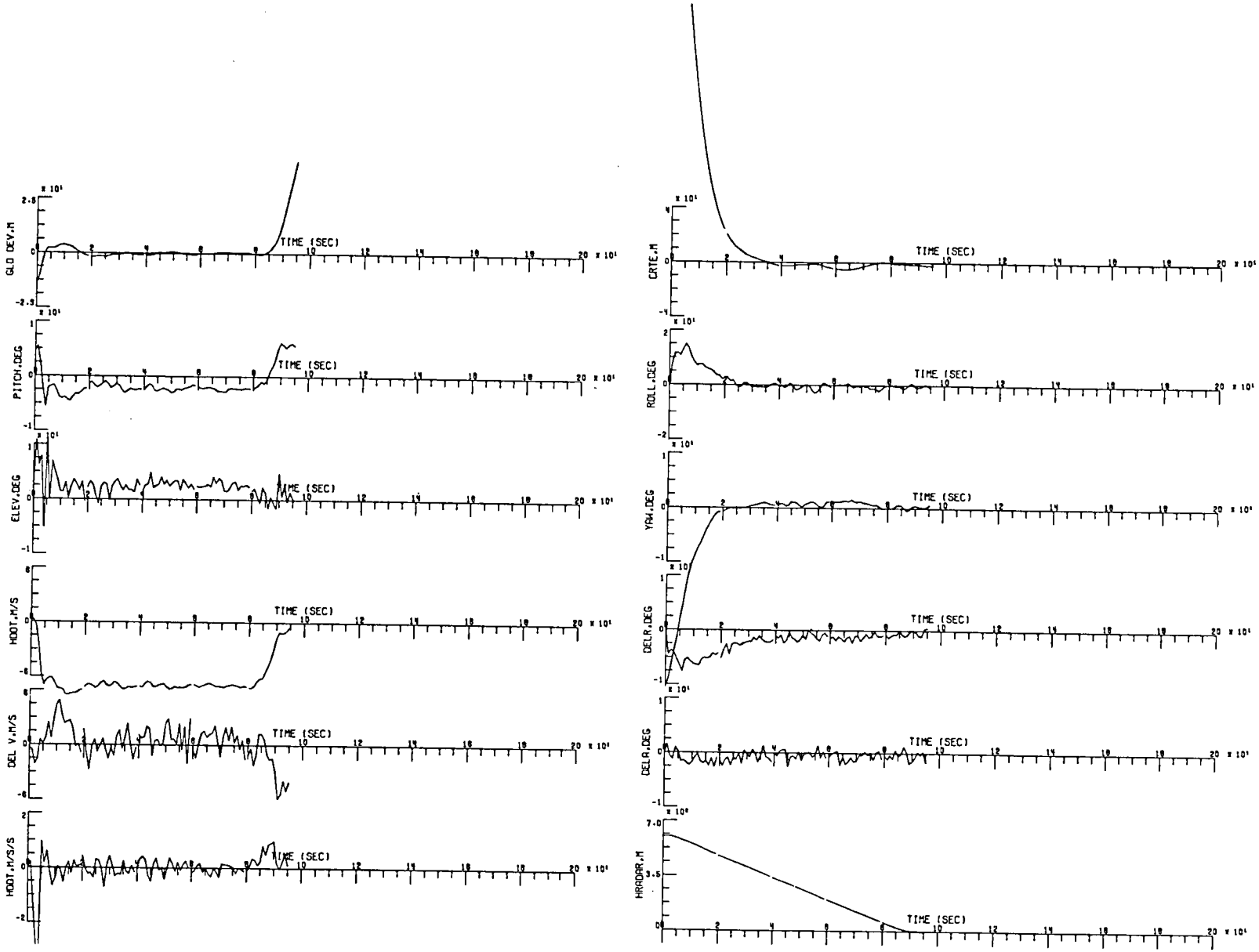

Figure 11 Final Approach Simulation: tail wind, average turbulence

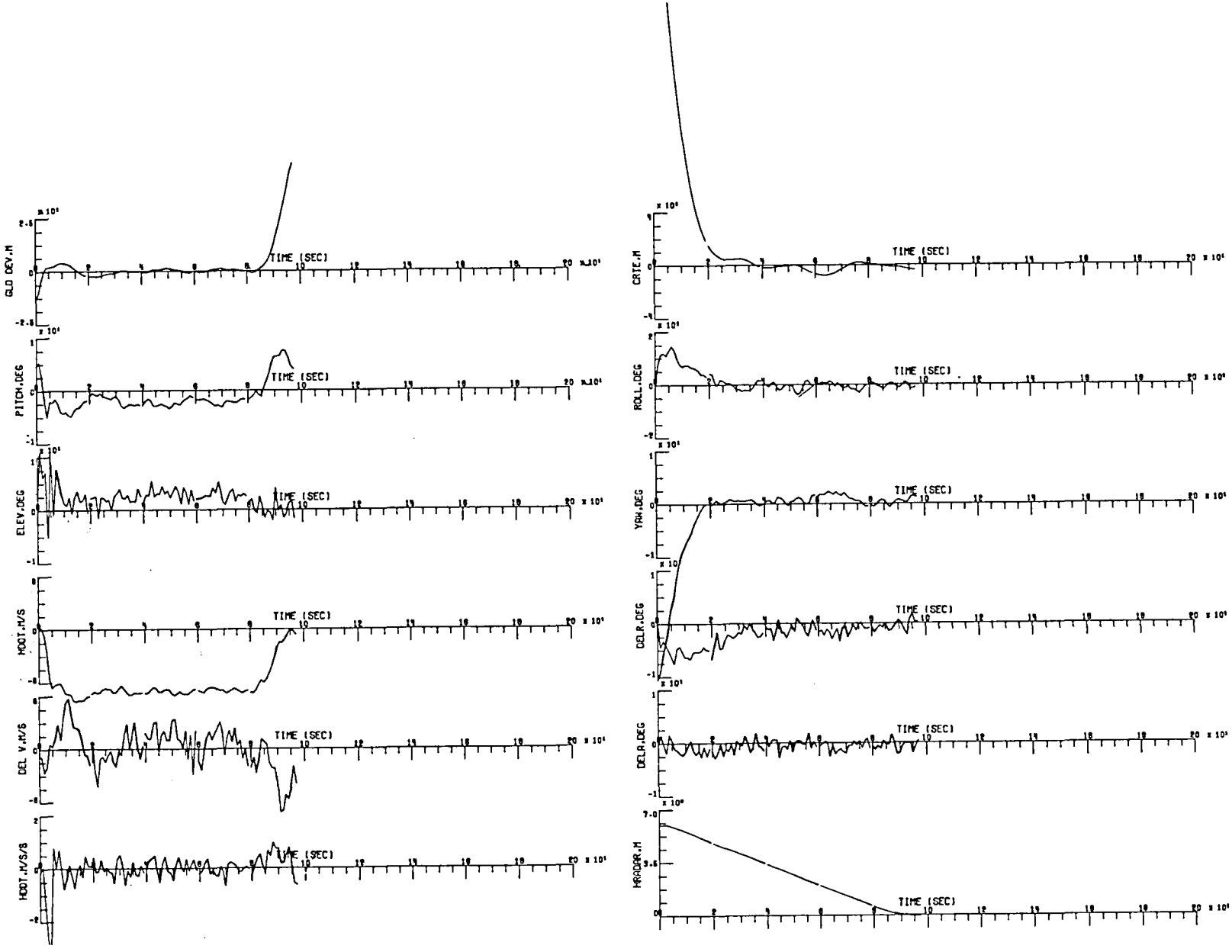

Figure 12 Final Approach Simulation: tail wind, high turbulence

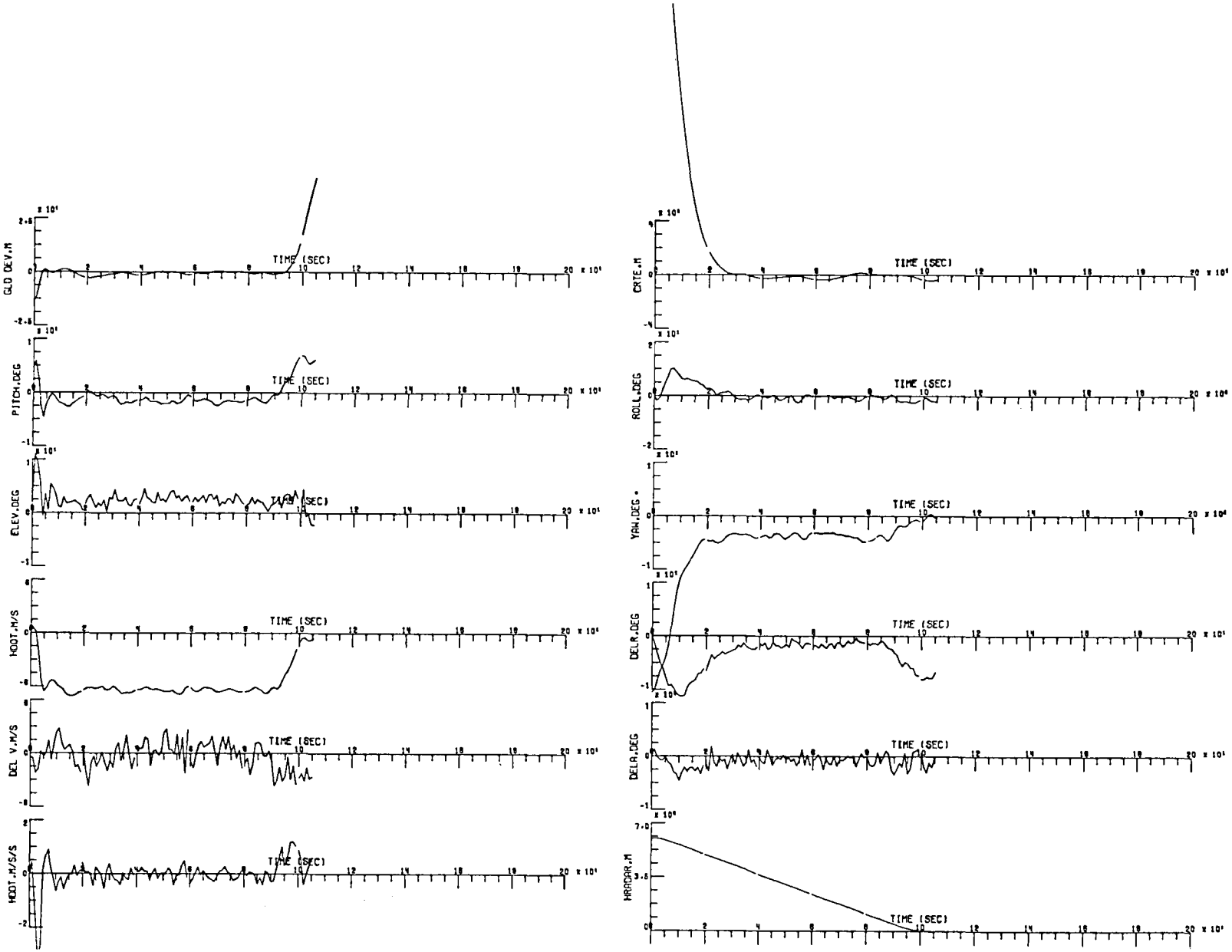

Figure 13 Final Approach Simulation: cross-wind, average turbulence

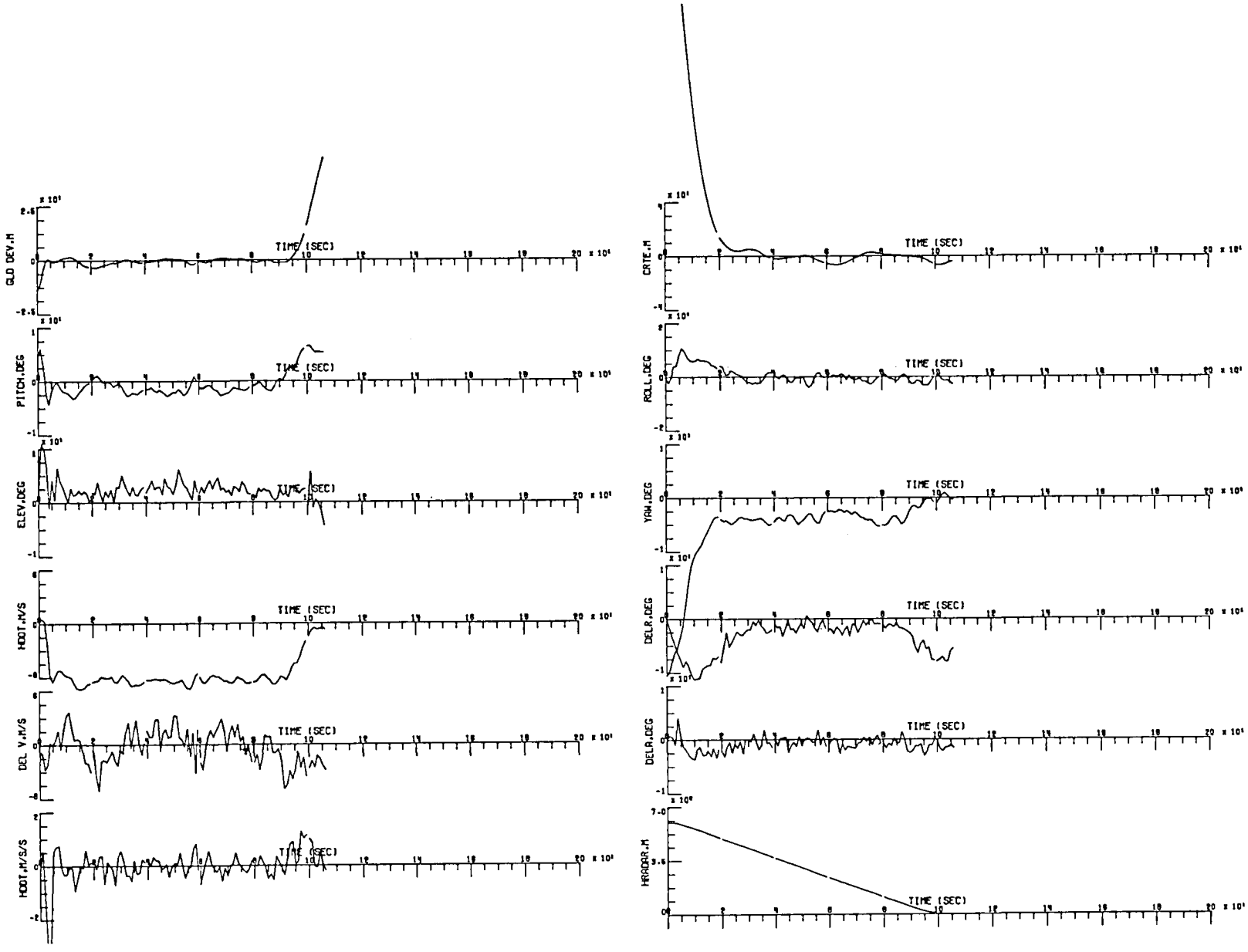

Figure 14 Final Approach Simulation: cross-wind, high turbulence

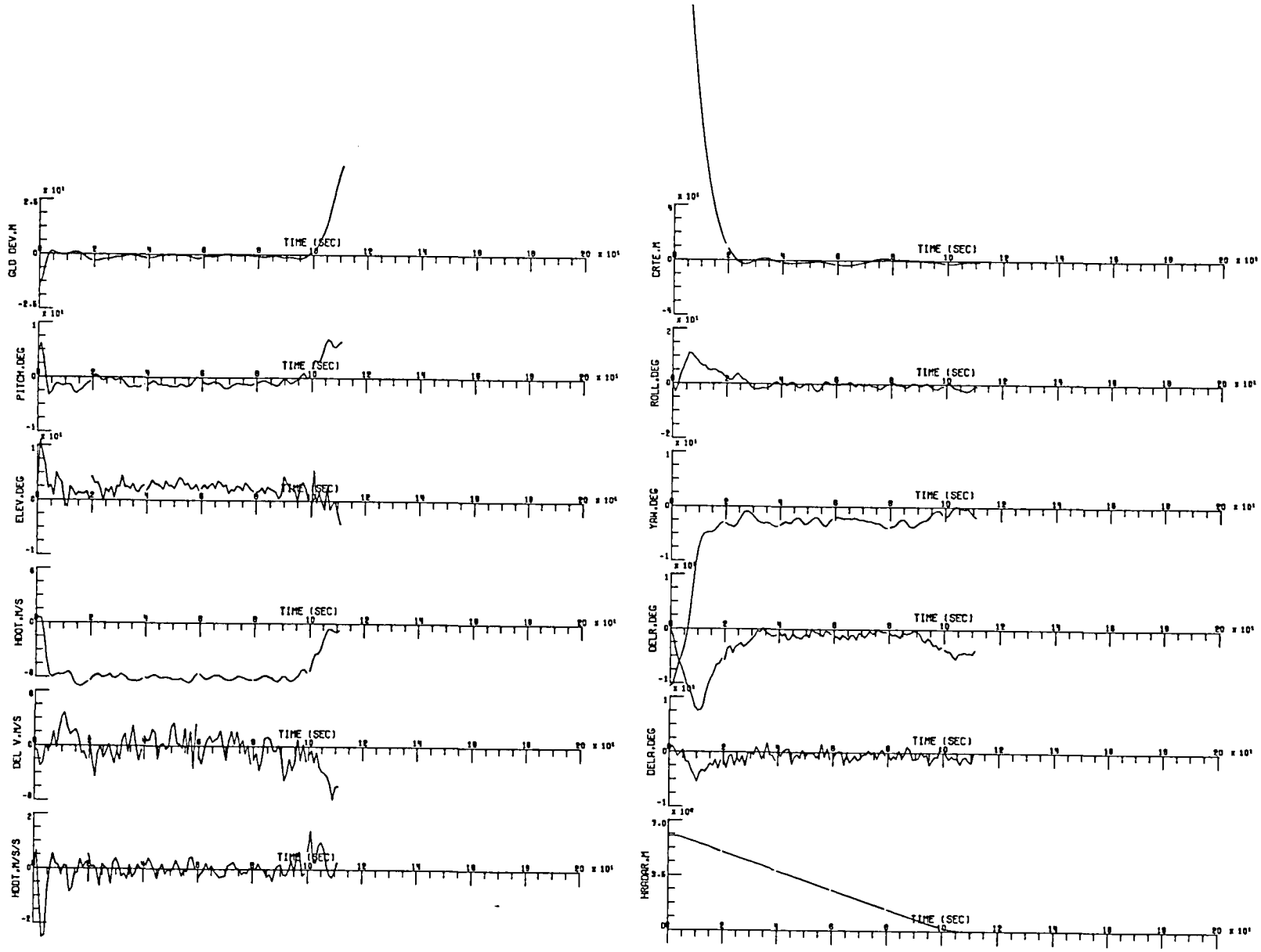

Figure 15 Final Approach Simulation: quartering headwind, average turbulence

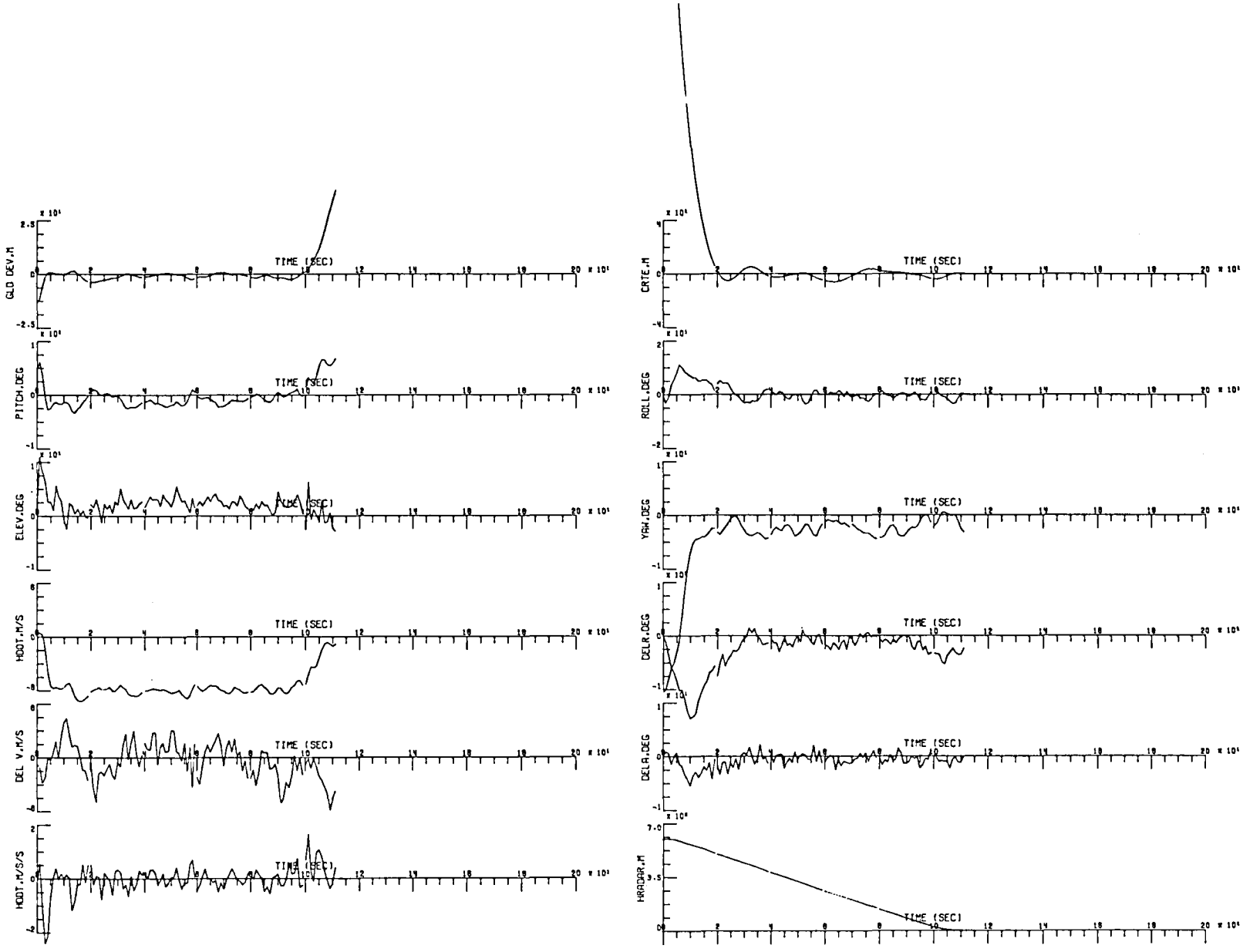

Figure 16 Final Approach Simulation: quartering headwind, high turbulence

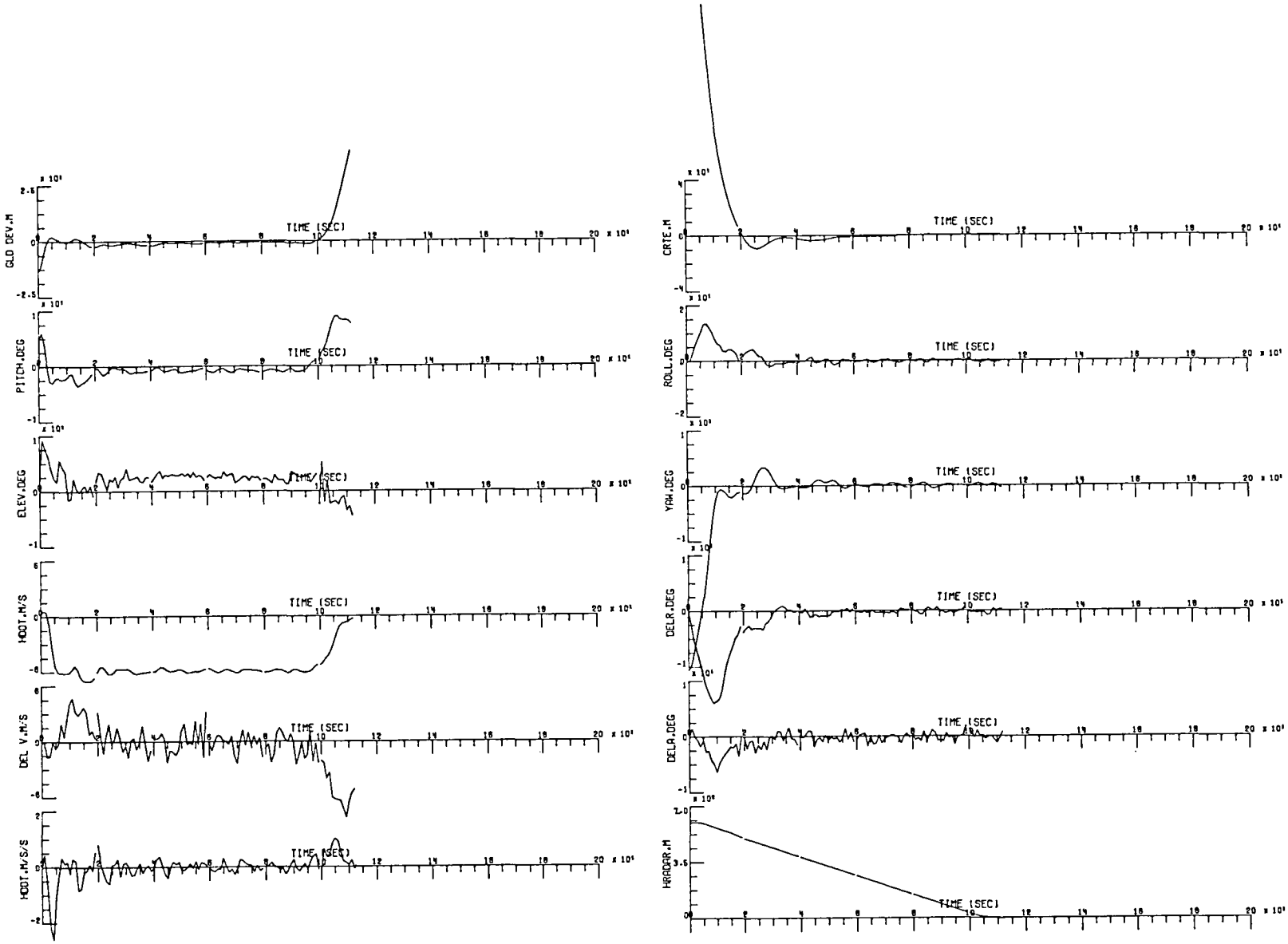

Figure 17 Final Approach Simulation: head wind with shear

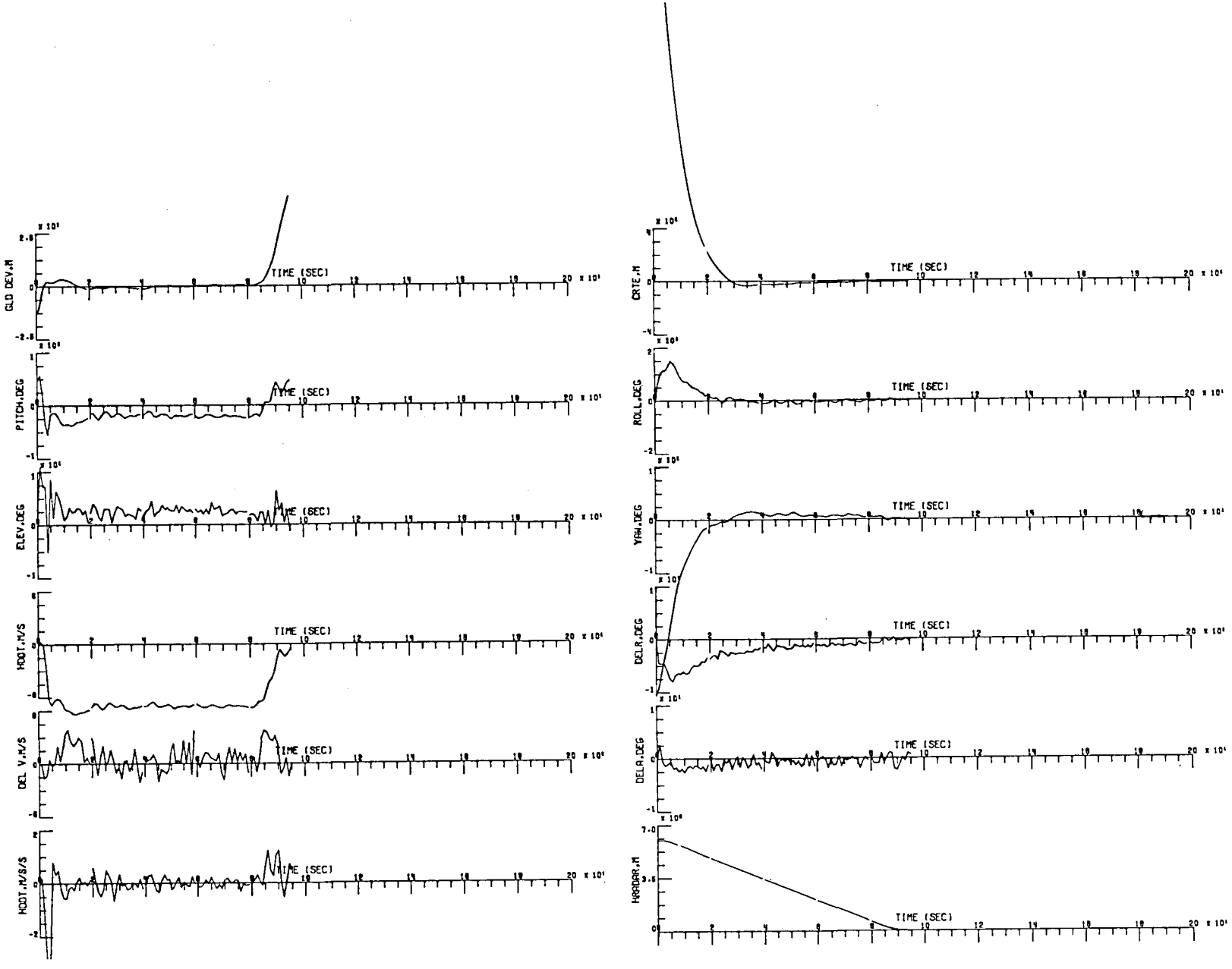

Figure 18 Final Approach Simulation: tail wind with shear

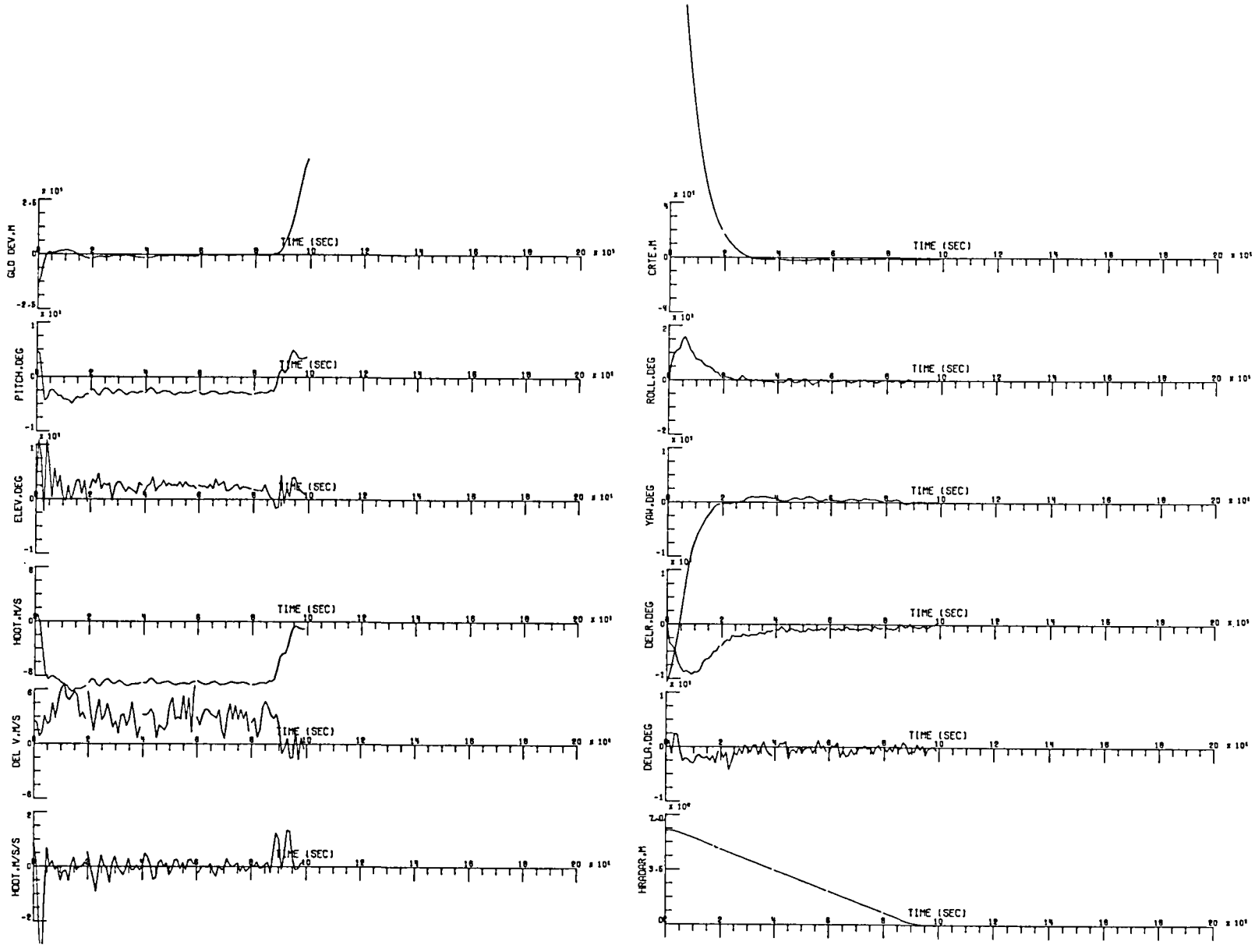

Figure 19 Final Approach Simulation: 64.3 m/sec (125 knot) airspeed

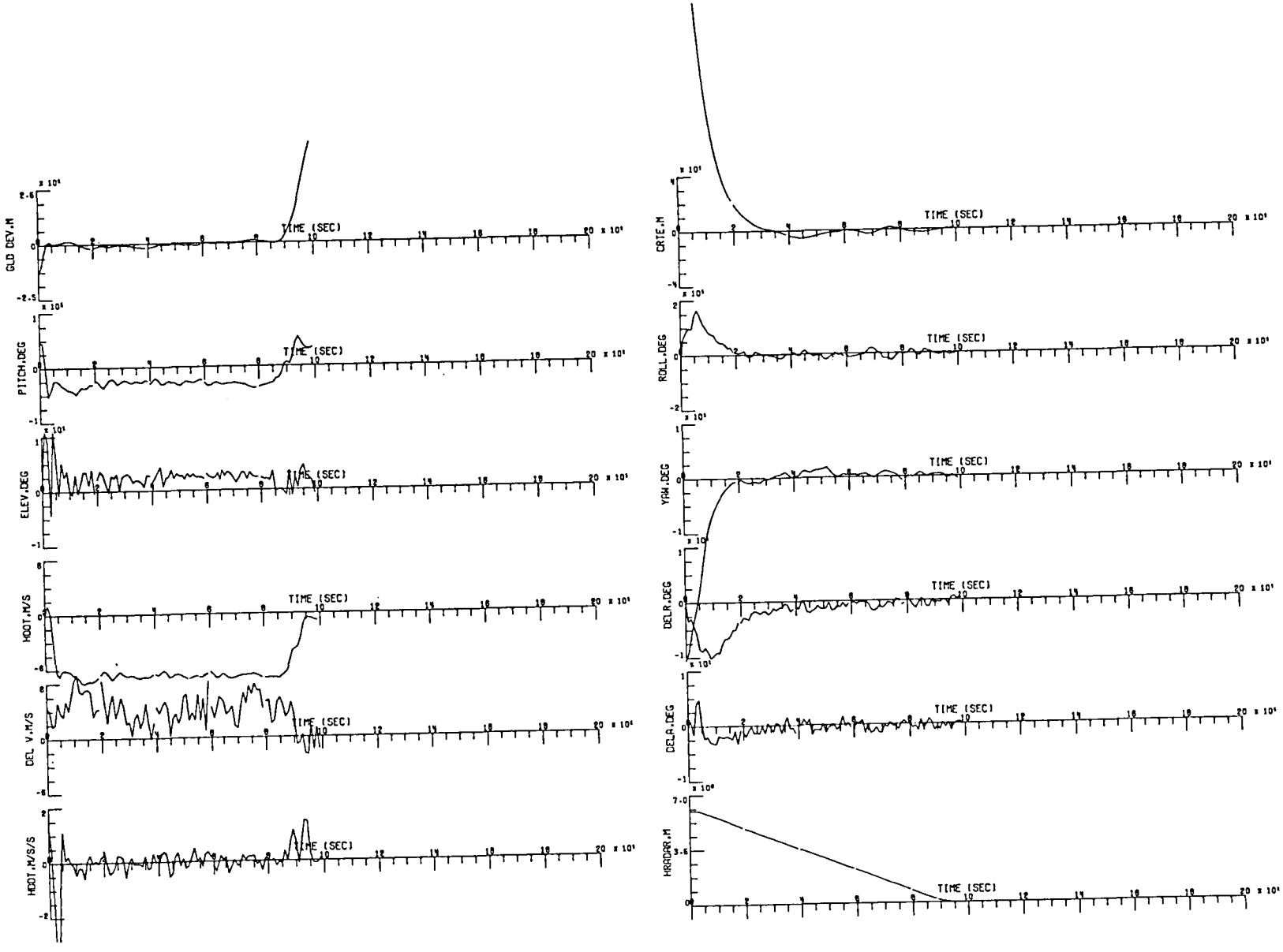

Figure 20 Final Approach Simulation: 64.3 m/sec (125 knot) airspeed, average gusts

TABLE 1 Sensor error model parameters

Sensor	Noise standard deviation	Bias	Comments
Attitude gyro	.229°	.229°	
Rate gyro	.02°/sec	0	
Body-mounted accelerometers	1% of g	1% of g	.229° misalignment and .25% scaling errors also modeled
MLS - azimuth	.01°	.0125°	jitter added
MLS - elevation	.01°	.0125°	jitter added
MLS - DME	2.29 m	2.29 m	
Radar altimeter	.305 m	.305 m	
Barometric altimeter	.305 m	1.52 m	
Barometric sink rate	.305 m/sec	.61 m/sec	
Airspeed indicator	2%	0	noise is multiplicative

$g = 9.81\ m/sec^2$

TABLE 2 Touchdown Statistics

Wind Conditions				Touchdown Conditions	
head wind (+) tail wind (-)	cross-wind	turbulence	shear	sink rate (m/sec)	deviation from average touch-down pt. (m)
0	0	0	F	.75	21.7
0	0	average	F	.91	25.3
0	0	high	F	1.08	31.4
+	0	0	F	.29	-4.5
+	0	average	F	.37	-32.6
+	0	high	F	.40	-64.6
-	0	0	F	.87	-21.0
-	0	average	F	.43	-9.1
-	0	high	F	.56	67.7
0	-	0	F	.84	-8.5
0	-	average	F	.60	2.19
0	-	high	F	.65	38.5
0	+	0	F	.39	-18.2
0	+	average	F	.75	47.0
0	+	high	F	1.27	54.9
+	-	0	F	.83	-28.3
+	-	average	F	.73	-26.2
+	-	high	F	.80	-38.7
+	0	0	T	.31	-31.7
-	0	0	T	.46	-12.4

average sink rate: .665 m/sec (2.18 ft/sec)

sink rate standard deviation: .26 m/sec (.85 ft/sec)

average touchdown point: 415.7 m (1363.8 ft)

standard deviation of touchdown point: 34.51 m (113.2 ft)

All steady winds have a magnitude of 5.14 m/sec (10 knots)

APPENDIX

The aircraft equations of motion given in section II are in state variable form. The relation of the elements of the matrices used in these equations to the stability derivatives of the aircraft are given here. The lateral equations are repeated here for convenience.

$$\dot{x} = Ax + Bu + Dw + \eta \quad , \tag{56}$$

$$\dot{W} = A_W \; W + B_W \; \omega \quad , \tag{57}$$

$$w = C_W \; W + \xi \quad . \tag{55}$$

The elements of the matrices in these equations are given below in terms of the aircraft's stability derivatives, and other aircraft parameters.

$$f_1 = \frac{I_{xx}}{q_o \, Sb} \quad , \qquad f_2 = \frac{I_{zz}}{q_o \, Sb} \quad , \qquad f_3 = \frac{I_{xz}}{q_o \, Sb} \quad ,$$

$$f_4 = f_1 \; f_2 - f_3^2 \quad , \quad f_5 = \frac{mU_o}{q_o S}$$

where S is the wing area, b the wing span, q_o the dynamic pressure, I_{xx}, I_{xz} and I_{zz} the aircraft's moments of inertia in stability axes, m the aircraft's mass

$$A_{14} = 1 \quad , \qquad A_{15} = \tan\theta_o \quad , \qquad A_{25} = \sec\theta_o \quad ,$$

$$A_{31} = \frac{\bar{g} \cos\theta_o}{U_o} \quad , \qquad A_{33} = \frac{C_{y\beta}}{f_5} \quad , \qquad A_{34} = \frac{C_{yp}}{f_5} \quad ,$$

$$A_{35} = \frac{C_{yr}}{f_5} - 1 \quad , \qquad A_{37} = \frac{C_{y\delta R}}{f_5} \quad ,$$

$$A_{43} = \frac{1}{f_4} \left[C_{\ell\beta} \; f_2 + f_3 \; (C_{n\beta} + C_{nT\beta}) \right] \quad ,$$

$$A_{44} = \frac{1}{f_4} \; (C_{\ell p} \; f_2 + f_3 \; C_{np}) \quad ,$$

$$A_{45} = \frac{1}{f_4} (C_{\ell r} \; f_2 + f_3 \; C_{nr}) \; , \quad A_{47} = \frac{1}{f_4} (C_{\ell \delta R} \; f_2 + f_3 \; C_{n\delta R}) \; ,$$

$$A_{53} = \frac{1}{f_2} (C_{n\beta} + C_{nT\beta} + f_3 \; A_{43}) \; , \quad A_{54} = \frac{1}{f_2} (C_{np} + f_3 \; A_{44}) \; ,$$

$$A_{55} = \frac{1}{f_2} (C_{nr} + f_3 \; A_{45}) \; , \quad A_{57} = \frac{1}{f_2} (C_{n\delta R} + f_3 \; A_{47}) \; ,$$

$$A_{61} = -\sin\alpha_0 \; , \quad A_{62} = \cos\gamma_0 \; , \quad A_{63} = 1 \; .$$

The elements of the matrix A for which an expression is not given above are zero; similarly, only non-zero elements of the remaining matrices will be given below.

$$B_{31} = \frac{1}{f_5} (C_{y\delta A} + c_{spa} \; C_{y\delta sp}) \; ,$$

$$B_{41} = \frac{1}{f_4} \left[(C_{\ell \delta A} \; f_2 + f_3 \; C_{n\delta A}) + c_{spa} \; (C_{\ell sp} \; f_2 + f_3 \; C_{n\delta sp}) \right]$$

$$B_{51} = \frac{1}{f_2} \left[C_{n\delta A} + \frac{f_3}{f_4} (C_{\ell \delta A} \; f_2 + f_3 \; C_{n\delta A}) + c_{spa} \left(C_{n\delta sp} + \frac{f_3}{f_4} (C_{\ell \delta sp} \; f_2 + f_3 \; C_{n\delta sp}) \right) \right] \; ,$$

$$B_{72} = 1 \; .$$

$$D_{31} = A_{33} \; , \quad D_{32} = A_{34} \; , \quad D_{33} = A_{35} \; ,$$

$$D_{41} = A_{43} \; , \quad D_{42} = A_{44} \; , \quad D_{43} = A_{45} \; ,$$

$$D_{51} = A_{53} \; , \quad D_{52} = A_{54} \; , \quad D_{53} = A_{55} \; .$$

The parameters related to the lateral wind model are given below.

$$A_{W12} = 1 \; ,$$

$$A_{W21} = -\left(\frac{U_0}{Lv} \right)^2 \; , \quad A_{W23} = -\frac{2U_0}{Lv} \; ,$$

$$A_{W32} = -\frac{\pi U_0}{3b} \quad , \quad A_{W33} = -\frac{\pi U_0}{3b} \quad ,$$

$$A_{W44} = -\frac{\pi U_0}{4b} \quad ,$$

$$A_{W56} = 1 \quad .$$

$$B_{W11} = -\sigma_V \sqrt{\frac{3}{\pi U_0 L_V}} \quad ,$$

$$B_{W21} = \sigma_V (2\sqrt{3} - 1 \sqrt{\frac{U_0}{\pi L^3_V}} \quad ,$$

$$B_{W31} = \frac{\sigma_V}{b} \sqrt{\frac{\pi U_0}{3 L_V}} \quad ,$$

$$B_{W42} = \frac{\sigma_W \pi}{4b} \sqrt{.8 \frac{U_0}{L_W} \left(\frac{\pi L_W}{4b} \right)^{\frac{1}{3}}} \quad ,$$

$$B_{W53} = 1 \quad , \quad B_{W54} = 1 \quad .$$

$$C_{W11} = 1 \quad , \quad C_{W15} = 1 \quad ,$$

$$C_{W23} = \sin\alpha_0 \quad , \quad C_{W24} = \cos\alpha_0$$

$$C_{W33} = \cos\alpha_0 \quad , \quad C_{W34} = -\sin\alpha_0 \quad .$$

The aircraft's longitudinal equations of motion were given in (37), and are repeated here along with the wind model for the longitudinal components of the wind velocities

$$\dot{x}_\ell = A_\ell x_\ell + B_\ell u_\ell + D_\ell w_\ell + \eta_\ell \qquad (37)$$

$$\dot{W}_\ell = A_{W\ell} W_\ell + \xi_\ell \quad , \quad w_\ell = C_{W\ell} W_\ell \quad . \qquad (68)$$

The elements of the matrices involved are given below in terms of the stability derivatives and the following intermediate parameters.

$$\alpha_1 = -\frac{mg\cos\theta_o}{q_o S} \quad , \qquad \alpha_2 = -\frac{mg\sin\theta_o}{q_o S}$$

$$\alpha_3 = \frac{mU_o}{q_o S} \quad , \qquad \alpha_4 = 1/(\alpha_3 + C_{L\dot{\alpha}}) \quad ,$$

$$\alpha_5 = I_{yy}/q_o S\bar{c} \quad , \qquad q_o = \tfrac{1}{2}\rho U_o^2 \quad ,$$

where S is the wing area, $\bar{c}$ the mean aerodynamics chord and ρ is the air density. Using these variables, the matrix elements are given below.

$$a_{\ell 14} = 1$$

$$a_{\ell 21} = \frac{\alpha_1}{\alpha_3} \quad , \quad a_{\ell 22} = \frac{1}{\alpha_3}(-C_{Du} - 2C_{Do} + C_{Txu} + 2C_{Txo}) \quad ,$$

$$a_{\ell 23} = \frac{-C_{D\alpha} + C_{Lo}}{\alpha_3} \quad , \quad a_{\ell 27} = \frac{C_{Tx}}{\alpha_3} \quad , \quad a_{\ell 28} = -\frac{C_{D\delta s}}{\alpha_3} \quad ,$$

$$a_{\ell 31} = \alpha_2\alpha_4 \quad , \quad a_{\ell 32} = -\alpha_4(C_{Lu} + 2C_{Lo}) \quad , \quad a_{\ell 33} = -\alpha_4(C_{L\alpha} + C_{Do}) \quad ,$$

$$a_{\ell 34} = \alpha_4(\alpha_3 - C_{Lq}) \quad , \quad a_{\ell 37} = \alpha_4 C_{Tz} \quad , \quad a_{\ell 39} = -\alpha_4 C_{L\delta s}$$

$$a_{\ell 41} = \alpha_4 C_{m\dot{\alpha}}\alpha_2/\alpha_5 \quad , \quad a_{\ell 42} = \frac{1}{\alpha_5}(C_{mu} + 2C_{mo} + C_{m\dot{\alpha}} a_{\ell 32}) \quad ,$$

$$a_{\ell 43} = \frac{1}{\alpha_5}(C_{m\alpha} + C_{mT\alpha} + C_{m\dot{\alpha}} a_{\ell 33}) \quad , \quad a_{\ell 44} = \frac{1}{\alpha_5}(C_{mq} + C_{m\dot{\alpha}} a_{\ell 34}) \quad ,$$

$$a_{\ell 47} = \frac{C_{mT} + C_{m\dot{\alpha}} a_{\ell 37}}{\alpha_5} \quad , \quad a_{\ell 49} = \frac{C_{m\delta s} + C_{m\dot{\alpha}} a_{\ell 49}}{\alpha_5}$$

$$a_{\ell 77} = .5 \quad , \quad a_{\ell 78} = .298;$$

$$b_{\ell 21} = -\frac{C_{D\delta e}}{\alpha_3} \quad , \quad b_{\ell 31} = -\alpha_4 C_{L\delta e} \quad , \quad b_{\ell 41} = \frac{C_{m\delta e} + C_{m\dot{\alpha}} b_{\ell 31}}{\alpha_5} \quad ;$$

$$d_{\ell 21} = a_{\ell 22} \quad , \quad d_{\ell 22} = a_{\ell 23} \quad ,$$

$$d_{\ell 31} = a_{\ell 32} \quad , \quad d_{\ell 32} = a_{\ell 33} \quad , \quad d_{\ell 33} = \alpha_4(C_{\ell\dot{\alpha}} - C_{Lq}) \quad ,$$

$$d_{\ell 41} = a_{\ell 42} \quad , \quad d_{\ell 42} = a_{\ell 43} \quad , \quad d_{\ell 43} = \frac{C_{mq} + (d_{\ell 33} - 1) C_{m\dot{\alpha}}}{\alpha_5} \quad .$$

$$A_{w\ell 12} = 1 \quad ,$$

$$A_{w\ell 21} = -\left(\frac{U_o}{L_w}\right)^2 \quad , \quad A_{w\ell 22} = -\frac{2\,U_o}{L_w}$$

$$A_{w\ell 31} = \frac{\pi\,U_o}{4b} \quad , \quad A_{w\ell 33} = \frac{-\pi\,U_o}{4b} \quad ,$$

$$A_{w\ell 44} = -\frac{U_o}{L_u} \quad , \quad A_{w\ell 57} = 1 \quad .$$

$$B_{w\ell 11} = \frac{\sqrt{3}\;U_o}{L_w} \quad ,$$

$$B_{w\ell 21} = (1 - \sqrt{12})\left(\frac{U_o}{L_w}\right)^2 \quad ,$$

$$B_{w\ell 72} = \frac{U_o}{L_w} \quad ,$$

$$B_{w\ell 64} = 1 \quad , \quad B_{w\ell 73} = 1 \quad .$$

$$C_{w\ell 11} = -\sin\alpha_o \quad , \quad C_{w\ell 14} = \cos\alpha_o \quad ,$$

$$C_{w\ell 15} = -\cos\gamma_o \quad , \quad C_{w\ell 16} = \sin\gamma_o \quad ,$$

$$C_{w\ell 21} = -\cos\alpha_o \quad , \quad C_{w\ell 24} = \sin\alpha_o \quad ,$$

$$C_{w\ell 25} = -\sin\gamma_o \quad , \quad C_{w\ell 26} = -\cos\gamma_o$$

$$C_{w\ell 31} = -\frac{\pi\,U_o}{4b} \quad , \quad C_{w\ell 33} = \frac{\pi\,U_o}{4b} \quad .$$

REFERENCES

1. Reeder, J. P., R. T. Taylor, and T. M. Walsh, "New designs and operating techniques for improved terminal area compatability," SAE, Air Transportation Meeting, Dallas, Texas, April 30, 1974.

2. Anon., "A new guidance system for approach and landing," vol. 2, Radio Technical Commission for Aeronautics, 1717 H Street N.W., Washington D. C., Document CO-148, Dec. 18, 1970.

3. B. Etkin, Dynamics of Atmospheric Flight, John Wiley & Sons, Inc., New York, 1972.

4. J. Roskam, Flight Dynamics of Rigid and Elastic Airplanes, Roskam Aviation and Engineering Corp., 519 Boulder, Lawrence, Kansas, 1972.

5. D. McRuer, I. Ashkenas, D. Graham, Aircraft Dynamics and Automatic Control, Princeton University Press, Princeton, New Jersey, 1973.

6. H. W. Bode and C. E. Shannon, "A simplified derivation of linear least-squares smoothing and prediction theory," Proc. IRE, vol. 38, pp. 417-425, April 1950.

7. B. D. O. Anderson, J. B. Moore and S. B. Loo, "Spectral factorization of time varying covariance functions," IEEE Trans. on info. theo., vol. IT-15, pp. 550-557, Sept. 1959.

8. N. Halyo and G. A. McAlpine, "On the spectral factorization of non-stationary vector random processes," IEEE Trans. on Automatic Control, vol. AC-19, No. 6, pp. 674-679.

9. C. R. Chalk, T. P. Neal, T. M. Harris and E. F. Prichard, "Background information and user guide for MIL-F-8785B (ASG), 'Military specification-flying qualities of piloted airplanes'," Air Force Flight Dynamics Report AFFDL-TR-69-72, Aug. 1969.

10. N. Halyo, "Development of an optimal automatic control law and filter algorithm for steep glideslope capture and glideslope tracking," NASA CR-2720, Aug. 1976.

11. N. Halyo, "Development of a digital automatic control law for steep glide-slope capture and flare," NASA CR-2834, June 1977.

12. J. A. Sorensen, "Analysis of instrumentation error effects on the identification of aircraft parameters," NASA CR-112121, 1972.

13. W. C. Hoffman, W. M. Hollister and R. W. Simpson, "Functional error analysis and modelling for ATC system concepts evaluation," DOT-TSC-72-1, May 1972.

14. K. Ogata, State space analysis of control systems, Prentice Hall, New Jersey, 1967.

15. N. Halyo and A. K. Caglayan, "A separation theorem for the stochastic sampled-data LQG problem," International J. of Control, vol. 23, No. 2, pp. 237-244, Feb. 1976.

16. D. E. Kirk, Optimal control theory: an introduction, Prentice Hall, Inc., Englewood Cliffs, New Jersey, 1970.

17. N. Halyo and R. E. Foulkes, "On the quadratic sampled-data regulator with unstable random disturbances, " IEEE SMC Soc. Proc., 1974 International Conf. on Syst., Man and Cybern., pp. 99-103, Oct. 1974.

18. S. Pines, S. F. Schmidt, F. Mann, "Automated landing, rollout and turnoff using MLS and magnetic cable sensors," NASA CR-2907, October 1977.

19. S. Pines, S. F. Schmidt, F. Mann, "Simulation, guidance and navigation of the B-737 for rollout and turnoff using MLS measurements," NASA CR-144959, Dec. 1975.

20. S. F. Schmidt, "A conceptual CTOL navigation system for curved-descending-decelerating approaches, " Anal. Mech. Assoc., Report No. 75-1, Jan. 1975.

1. Report No.	2. Government Accession No.	3. Recipient's Catalog No.
NASA CR-3074		

4. Title and Subtitle	5. Report Date
Development of a Digital Guidance and Control Law for Steep Approach Automatic Landings Using Modern Control Techniques	February 1979
	6. Performing Organization Code
7. Author(s)	8. Performing Organization Report No.
Nesim Halyo	AMA No. 77-24
	10. Work Unit No.
9. Performing Organization Name and Address	
Analytical Mechanics Associates, Inc. 17 Research Road Hampton, VA 23666	11. Contract or Grant No. NAS1-14088
	13. Type of Report and Period Covered
12. Sponsoring Agency Name and Address	Contractor Report
National Aeronautics and Space Administration Washington, DC 20546	14. Sponsoring Agency Code

15. Supplementary Notes

Langley Technical Monitor: Richard M. Hueschen
Final Report

16. Abstract

This report contains the development of a digital automatic control law for a small jet transport to perform a steep final approach in automatic landings. It also contains the development of a steady-state Kalman filter used to provide smooth estimates to the control law. The control law performs the functions of localizer and glideslope capture, localizer and glideslope track, decrab, and place. The control law uses the Microwave Landing System (MLS) position data, and aircraft body-mounted accelerometers, attitude and attitude rate information.

The results obtained from a digital simulation of the aircraft dynamics, wind conditions, and sensor noises using the control law and filter developed are described.

17. Key Words (Suggested by Author(s))	18. Distribution Statement
Automatic Landing Digital Guidance and Control Steep Approach, Microwave Landing System (MLS) Kalman Filter Digital Simulation	Unclassified - Unlimited Subject Category 17

19. Security Classif. (of this report)	20. Security Classif. (of this page)	21. No. of Pages	22. Price*
Unclassified	Unclassified	70	$5.25

* For sale by the National Technical Information Service, Springfield, Virginia 22161

NASA-Langley, 1979

National Aeronautics and
Space Administration

Washington, D.C.
20546

Official Business
Penalty for Private Use, $300

THIRD-CLASS BULK RATE

Postage and Fees Paid
National Aeronautics and
Space Administration
NASA-451

U.S.MAIL

NASA

POSTMASTER: If Undeliverable (Section 158 Postal Manual) Do Not Return